JOURNAL OF MAGNETIC RESONANCE **134,** 261–279 (1998)
ARTICLE NO. MN981506

Direct Determination of Motional Correlation Times by 1D MAS and 2D Exchange NMR Techniques

D. E. Favre, D. J. Schaefer,[1] and B. F. Chmelka[2]

Department of Chemical Engineering, University of California, Santa Barbara, California 93106

Received March 6, 1998

One- and two-dimensional static and magic-angle spinning (MAS) exchange NMR experiments for quantifying slow (τ_c > 1 ms) molecular reorientation dynamics are analyzed, emphasizing the extent to which motional correlation times can be extracted *directly* from the experimental data. The static two-dimensional (2D) exchange NMR experiment provides geometric information, as well as exchange time scales via straightforward and model-free application of Legendre-type orientational autocorrelation functions, particularly for axially symmetric interaction tensors, as often encountered in solid-state ^{2}H and ^{13}C NMR. Under conditions of MAS, increased sensitivity yields higher signal-to-noise spectra, with concomitant improvement in the precision and speed of correlation time measurements, although at the expense of reduced angular (geometric) resolution. For random jump motions, one-dimensional (1D) *e*xchange-*i*nduced *s*idebands (EIS) ^{13}C NMR and the recently developed ODESSA and time-reverse ODESSA experiments complement the static and MAS two-dimensional exchange NMR experiments by providing faster means of obtaining motional correlation times. For each of these experiments, the correlation time of a dynamic process may be obtained from a simple exponential fit to the integrated peak intensities measured as a function of mixing time. This is demonstrated on polycrystalline dimethylsulfone, where the reorientation rates from EIS, ODESSA, time-reverse ODESSA, and 2D exchange are shown to be equivalent and consistent with literature values. In the analysis, the advantages and limitations of the different methods are compared and discussed.

Key Words: **exchange NMR; EIS; ODESSA; motional correlation times; dimethylsulfone.**

INTRODUCTION

Static (i.e., nonspinning) and rotor-synchronized MAS two-dimensional (2D) exchange NMR experiments have been extensively used to study slow reorientational dynamics in solid-state materials for motional time scales ranging from milliseconds to seconds (*1–5*). However, these 2D methods can be exceedingly time-consuming. For random jump motions, the one-dimensional (1D) MAS methods of *e*xchange-*i*nduced *s*idebands (EIS) (*6, 7*), *o*ne-*d*imensional *e*xchange *s*pectroscopy by *s*ideband *a*lternation (ODESSA) (*8*), and "time-reverse" ODESSA (*9*) complement the 2D exchange experiments; while sacrificing geometric resolution, these 1D MAS exchange experiments provide faster means of obtaining motional correlation times without the need to determine explicitly longitudinal (T_1) relaxation times, as will be shown later. This represents a significant advantage to the direct measurement of time scales associated with slow dynamic molecular processes. After a brief account of the various exchange techniques available, a detailed description of the EIS experiment will be given, illustrating how motional correlation times may be extracted directly from experimental data. This leads to insightful comparisons with analyses of 2D exchange, ODESSA, and time-reverse ODESSA spectra, from which it will be shown that direct extraction of motional correlation times is also possible.

Each of the different solid-state exchange NMR methods is based on the dependence of the NMR frequency on the orientation of the principal axes system (PAS) of the nuclear spin interaction tensor relative to the static magnetic field $\mathbf{B}_0$ (*1*). Two-dimensional exchange NMR monitors changes in these angular-dependent NMR frequencies occurring during a mixing time (t_m) by correlating the frequencies in the evolution (t_1) and detection (t_2) periods, which bracket the mixing time; see Fig. 1a. Changes in the NMR frequencies manifest themselves as off-diagonal intensity in the 2D exchange spectrum $S(\omega_1, \omega_2; t_m)$, which can be regarded as a correlation map of the frequencies measured in the evolution and detection periods, ω_1 and ω_2, respectively, and which parametrically depends on the mixing time t_m. In other words, the two-dimensional spectrum $S(\omega_1, \omega_2; t_m)$ represents the joint probability density of finding a certain PAS orientation with respect to the external magnetic field, and thus a certain NMR frequency ω_1 during the evolution period t_1, and, after a time interval t_m later, finding the same PAS with a NMR frequency ω_2 during the detection period t_2 (*10*). Fast magic-angle sample spinning averages the anisotropies of these interactions, resulting in higher-resolution NMR spectra with peaks at the positions of the isotropic chemical shift values. Under such circumstances, chemical exchange or conformational transitions are detected

[1] Current address: Symyx Technologies, Santa Clara, CA 95051.
[2] To whom correspondence should be addressed. Fax: (805) 893 4731. E-mail: bradc@engineering.ucsb.edu.

1090-7807/98 $25.00

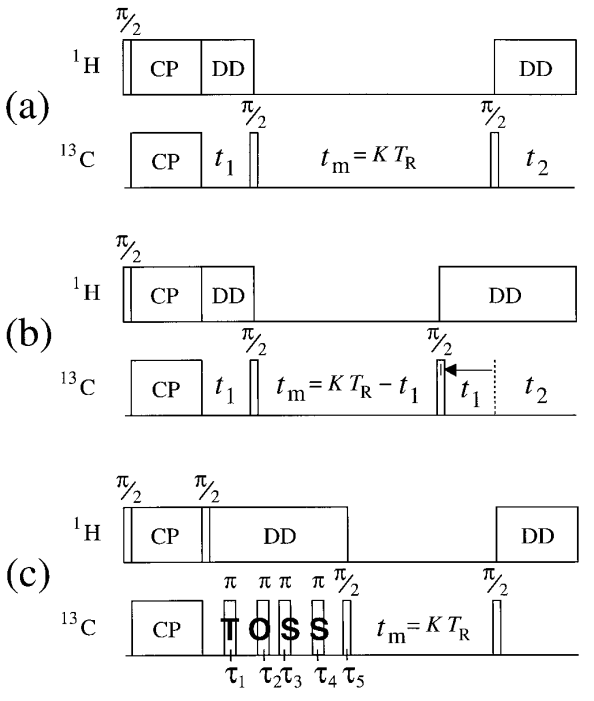

FIG. 1. Schematic diagrams of the pulse sequences used for exchange ^{13}C NMR experiments. (a) Static and MAS 2D exchange and ODESSA experiments. Transverse proton magnetization created by a $\pi/2$ pulse is transferred to ^{13}C by cross-polarization (CP); the information about the NMR frequencies during the subsequent evolution time t_1 is stored along the z-axis by the first ^{13}C $\pi/2$-pulse, which initiates the mixing time t_m. Molecular reorientations can take place during the mixing period, thereby altering the NMR frequencies, which are measured in the detection time t_2 after the second $\pi/2$-pulse. A refocusing $\pi/2$-pulse can be used to create a Hahn echo in the detection period. High-power proton dipolar decoupling (DD) is applied to remove heteronuclear ^{1}H–^{13}C dipolar couplings during t_1 and t_2. For the MAS and static 2D exchange NMR experiments, a two-dimensional data set $F(t_1, t_2; t_m)$ is generated by repeating the experiment with incremented values of the evolution time t_1 while keeping t_m constant. For rotor-synchronized MAS 2D exchange and ODESSA, the additional requirement $t_m = KT_R$ (where K is an integer and T_R is the rotor period) must be fulfilled. For ODESSA, t_1 is set to half a rotor period. (b) Pulse sequence for time-reverse ODESSA; t_1 is set to half a rotor period, and the mixing time is rotor-synchronized to be a half-integral number of rotor periods. Acquisition starts one-half rotor period after the mixing time t_m. The same pulse sequence is used for rotor-synchronized MAS 2D exchange, except signal acquisition begins immediately after the final $\pi/2$-pulse. (c) Pulse sequence for the EIS experiment. A TOSS sequence is used to suppress spinning sidebands during the preparation period, followed by a mixing time t_m lasting an integral number of rotor periods.

as cross peaks in non-rotor-synchronized MAS 2D exchange NMR spectra (*11, 12*). This can also be achieved at modest spinning speeds by applying a combination of a TOSS (*to*tal suppression of *s*idebands) (*13*) and time-reverse TOSS pulse sequences in the evolution and detection periods of a two-dimensional exchange NMR experiment to effect evolution under the isotropic chemical shift alone (*14*), or by chemical shift scaling techniques (*15*).

Whereas information on geometrical aspects of slow ($\tau_c > 1$ ms) jump-type reorientational processes can be obtained from a single static 2D exchange spectrum, information on the time scale of the process at any given temperature requires that a set of 2D exchange spectra be acquired as a function of the mixing time t_m. The time scale can be quantified directly from the experimental spectra by computing the rise of the ratios of off-diagonal intensity to overall intensity $R^{2D}(t_m)$ from each individual spectrum (in slices where diagonal and off-diagonal intensities are well separated), by calculating the time-dependent second-order orientational autocorrelation function $C_2(t_m) = \langle \omega(0)\omega(t_m)\rangle = \langle \omega_1\omega_2\rangle(t_m) = \int d\omega_1 \int d\omega_2 S(\omega_1, \omega_2; t_m)\omega_1\omega_2$ (*1, 16*), or by following the loss of correlation from the decrease of the echo intensity of the 2D exchange time-domain signal for selected values of the evolution time t_1 as a function of the mixing time (*17*). The latter provides complementary information to the 2D exchange experiment, because the echo intensity is related to the diagonal fraction of the 2D exchange spectrum and can be used to probe the decrease of the spectral diagonal in favor of off-diagonal exchange intensity.

In quantifying an elementary dynamic process, an activation energy is often sought, which requires determination of the temperature dependence of the respective motional correlation times. This entails the acquisition of series of high-signal-to-noise-ratio 2D exchange spectra with varying mixing times at different temperatures, which is typically time-consuming and often infeasible, especially in the case of dilute nuclei or for species with long spin–lattice relaxation times T_1. For example, one static 2D exchange ^{13}C NMR spectrum of benzene, 99% ^{13}C enriched at a single ring site, adsorbed on Ca-LSX zeolite required 66 h of measurement time (*18*). Time requirements are high even if only the decay of the echo intensity in the time domain is followed for a few selected evolution times t_1. Furthermore, to extract precisely the motional correlation time, it is often necessary to correct for spin–lattice relaxation during the mixing time, which leads to a decrease in the overall signal intensity, so that T_1 should be known from independent measurements. Consequently, it is desirable to examine experimental techniques that yield improved sensitivity over the static 2D exchange experiment, thereby reducing the amount of time necessary to acquire a spectrum. Moreover, as will be shown, it is possible to achieve this while still preserving the direct extraction of time scale information for jump-type reorientation processes, without the need to determine the spin–lattice relaxation time T_1 explicitly.

A variety of techniques that are one-dimensional analogs of the static 2D exchange experiment exist for quantifying motional correlation times. For example, selective excitation has been used to select a narrow band of frequencies from an inhomogeneously broadened powder spectrum, after which molecular-motion-induced changes in the angle-dependent frequencies are detected in spectral intensity outside of the initially selected band of frequencies (*1*). Although only a one-dimensional experiment needs to be performed, the reduction of measurement time is marginal, because most of the signal is

suppressed by the selective excitation. Alternatively, selective inversion of a fraction of an inhomogeneously broadened powder lineshape is another one-dimensional analog to the 2D exchange experiment. This method, however, is applicable only to systems that do not experience rapid homogeneous signal decays, that is, short T_2 relaxation times (*19*). Similarly, selective inversion MAS techniques using, for example, the DANTE pulse sequence, can be used to invert selectively one family of spinning sidebands and monitor their return to equilibrium as a function of a mixing time (*19*). These techniques are experimentally demanding and are typically executed using specialized instrumentation often not available in commercial spectrometers (*19*).

The rotor-synchronized MAS 2D exchange NMR experiment is directly related to the static 2D exchange experiment in that it detects molecular reorientation as discrete cross peaks between different sidebands in the 2D plane (*2, 5*). Because four different two-dimensional time domain signals have to be acquired to obtain pure absorption mode spectra, i.e., two signals with the pulse sequence depicted in Fig. 1a and two signals yielding the time-reversed counterparts with the pulse sequence shown in Fig. 1b, the experiment is time-intensive to perform. It is therefore desirable to use, whenever possible, equivalent 1D methods.

The ODESSA experiment recently proposed by Tekely and co-workers is closely related to the rotor-synchronized MAS 2D exchange experiment (*8*). The same pulse sequence is used as for the 2D exchange experiment with a rotor-synchronized mixing time and with the evolution period fixed at a value $t_1 = T_R/2$ in the ODESSA experiment; see Fig. 1a. If no reorientation takes place during the mixing time, a MAS spectrum is obtained in which all of the odd-numbered sidebands are inverted. Dynamic processes during the mixing time result in a reduction in the overall intensity of the ODESSA spectrum and modification of the sideband patterns; see Fig. 2a. The ODESSA method works properly if the experiment is performed on-resonance and if only one isotropic chemical shift, and thus one family of sidebands, is present. These shortcomings are overcome in the time-reverse ODESSA experiment, which generates spectra with all families of sidebands in-phase, provided only the orientations associated with the nuclear spin interaction tensors change and the isotropic values remain constant (*9*). Here, too, the evolution time is fixed to half a rotation period, $t_1 = T_R/2$, the mixing time is set to an odd number of half rotor periods, $t_m = (2K - 1)T_R/2$, and, unlike the case of the time-reverse MAS 2D exchange signals, acquisition starts at $t_2 = T_R/2$ after the detection pulse; see Fig. 1b. As shown in Fig. 2b, in the absence of molecular reorientation dynamics, the time-reverse ODESSA spectrum resembles a normal MAS spectrum; however, when dynamics are present, the overall intensity of the time-reverse ODESSA spectrum is diminished, and the sideband patterns are modified. For both the ODESSA and time-reverse ODESSA experiments, it has been demonstrated that the time scale can be extracted directly from the experimental data (*8, 9*), provided

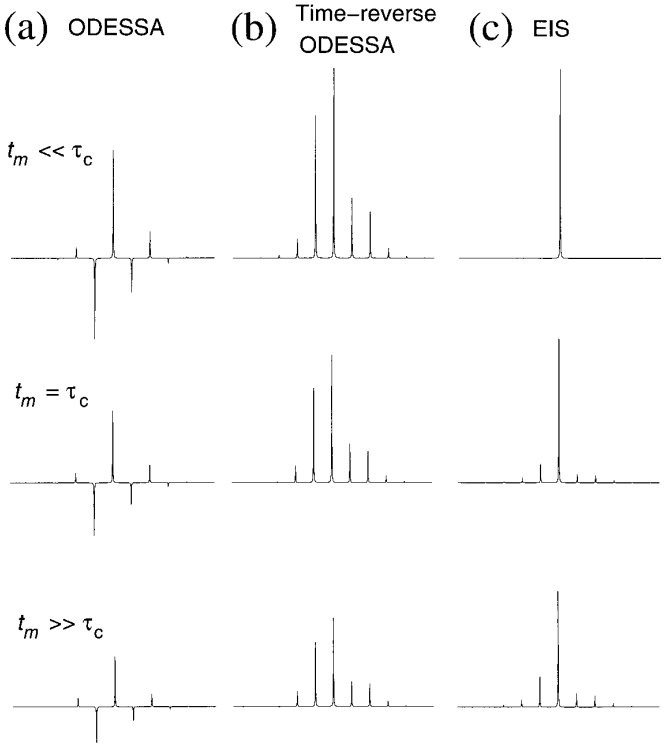

FIG. 2. Simulated ^{13}C NMR spectra for dimethylsulfone under the conditions of different 1D MAS exchange experiments for a spinning speed of $\omega_R = 2\pi \times 1800$ Hz, a ^{13}C frequency of 125.4 MHz, and the chemical shift tensor given in Ref. (*8*): $\sigma_{xx} = 63.5$, $\sigma_{yy} = 60.7$, and $\sigma_{zz} = 6.0$ ppm. Each series simulates no exchange ($t_m \ll \tau_c$), exchange when the mixing time equals the correlation time for the motion ($t_m = \tau_c$), and full exchange ($t_m \gg \tau_c$) for (a) ODESSA spectra, (b) time-reverse ODESSA spectra, and (c) EIS spectra. The spectra are normalized to the first spectrum in each series.

the T_1 relaxation time is known from independent measurements or obtained from a fit to the spectra (an unnecessary restriction, as will be shown later).

Another 1D exchange MAS method that is closely related to the 2D exchange experiment is the EIS technique, designed by Yang *et al.* (*6*). As will be shown later, EIS also permits motional correlation times to be extracted directly from the data without explicit determination of the longitudinal relaxation time T_1. In samples with an isotropic distribution of molecular orientations, the spinning sidebands can be suppressed through the use of the well-known TOSS pulse sequence, yielding only peaks at the positions of the respective isotropic chemical shifts in the 1D TOSS spectra; see Fig. 2c, top. As shown in Fig. 1c, the TOSS and the exchange NMR experiments can be combined by incorporating TOSS in the preparation period of an exchange experiment. This is followed by a mixing time during which molecular dynamics can occur and cause frequency changes that reintroduce sidebands in the 1D MAS spectrum acquired in the subsequent detection period; see Fig. 2c. This combined TOSS/exchange experiment constitutes the EIS technique (*6, 7*), in which simply the presence of sidebands provides evidence for frequency changes, such as

those produced by molecular motion; suppressed sidebands are restored as a result of molecular reorientation (or magnetization transfer via spin diffusion), which allows direct characterization of the associated time scale. Other spinning sideband suppression techniques can also be used instead of the TOSS sequence, for example, SELTICS (sideband *el*imination by *t*emporary *i*nterruption of the *c*hemical *s*hift) (*20*).

The EIS technique was first demonstrated on polycrystalline dimethylsulfone (DMS) (*6*); however, comparison with computer simulations of the spectra appeared to be necessary to yield motional time constants from the experimental data. The experiment was later applied to study spin diffusion in a dipotassium salt of α-glucopyranose-1-phosphate and in spider silk (*21*), but the data were analyzed in a manner that required the determination of spin–lattice relaxation times. As will be shown later, the experimental EIS data can be analyzed in terms of the ratio $R^{\mathrm{EIS}}(t_{\mathrm{m}})$ of combined sideband intensity to the total (sideband + centerband) intensity of the EIS spectrum, which is analogous to an analysis of static 2D exchange spectra using the off-diagonal-to-total intensity ratio $R^{2\mathrm{D}}(t_{\mathrm{m}})$. This work represents a first-time demonstration of the simple and direct extraction of motional correlation times for a single random-jump-type motion using EIS, expanding significantly the description given in the original papers (*6*, *7b*). Furthermore, these results will be shown to be closely related to the ODESSA, time-reverse ODESSA, and static 2D exchange experiments. We will demonstrate consistency among the results obtained from each of these exchange NMR techniques and other methods for quantifying molecular jump motions, specifically in dimethylsulfone.

THEORY

In the solid state, the NMR frequency depends on the orientation of a molecule in the external magnetic field $\mathbf{B}_0$ due to the anisotropy of the nuclear spin interactions, which are described by second-rank tensors (*1*, *22*). For the case of a spin $I = \frac{1}{2}$ nucleus possessing a chemical shift anisotropy (CSA), the angular dependence of the NMR frequency in the rotating frame is given by (*1*, *22*)

$$\omega(\alpha, \beta) = \omega_{\mathrm{iso}} + \tfrac{1}{2}\,\delta(3\cos^2\beta - 1 - \eta\sin^2\beta\cos(2\alpha)), \quad [1]$$

where ω_{iso} denotes the isotropic chemical shift frequency, δ specifies the coupling strength, and the asymmetry parameter η represents the deviation from axial symmetry about the z-axis of the chemical shift tensor $\underline{\underline{\sigma}}$; the polar angles α and β describe the orientation of the magnetic field $\mathbf{B}_0$ in the principal axes system (PAS) of the interaction tensor $\underline{\underline{\sigma}}^{\mathrm{PAS}}$. The principal axes system for the generally dominating intramolecular contributions is determined by the local symmetry of the molecule in the vicinity of the nucleus under study. In the case of an axially symmetric coupling tensor ($\eta = 0$), only the angle β between the z-principal axis of the coupling tensor and the external magnetic field $\mathbf{B}_0$ is relevant:

$$\omega(\beta) - \omega_{\mathrm{iso}} = \tfrac{1}{2}\,\delta(3\cos^2\beta - 1) = \delta P_2(\cos\beta), \quad [2]$$

where $P_2(\cos\beta)$ is the second-order Legendre polynomial. Note that in ^{2}H NMR, where the dominant interaction is between the electric field gradient (EFG) tensor and the nuclear electric quadrupole moment, the angular dependence is given by the same expressions Eq. [1] and Eq. [2], except for a "$\pm$" sign in front of the angle-dependent term, accounting for the two transitions of the spin $I = 1$ system.

MAS and TOSS

Sample rotation renders the orientation of each molecule with respect to the external magnetic field time-dependent, resulting in a time dependence of the NMR resonance frequency. In MAS NMR, sample rotation at a frequency $\omega_{\mathrm{R}} = 2\pi/T_{\mathrm{R}}$, where T_{R} is the period of rotation, can conveniently be described in a frame fixed with the sample rotor, called the rotor frame (RF), with the rotor axis as the z_{RF}-axis inclined at $\Theta_{\mathrm{m}} = 54.74°$ with respect to $\mathbf{B}_0$ and the time-dependent azimuthal angle given as $\omega_{\mathrm{R}}t$. This requires that the chemical shift interaction tensor $\underline{\underline{\sigma}}$, as well as the external magnetic field $\mathbf{B}_0$ that constitutes the z_{LF}-axis of the laboratory frame (LF), be expressed in the RF. Although $\underline{\underline{\sigma}}^{\mathrm{PAS}}$ can be converted directly into $\underline{\underline{\sigma}}^{\mathrm{RF}}$, it is often convenient to transform from the PAS via Euler angles (α', β', γ') to a molecular frame (MF), fixed to a local molecular segment, where molecular reorientation is more easily described. The transformation is then extended from the MF to the RF using the Euler angles (α, β, γ):

$$\mathrm{PAS},\ \underline{\underline{\sigma}}^{\mathrm{PAS}} \xrightarrow[\alpha',\beta',\gamma']{} \mathrm{MF}, \quad \underline{\underline{\sigma}}^{\mathrm{MF}} \xrightarrow[\alpha,\beta,\gamma]{} \mathrm{RF} \xleftarrow[0,\Theta_{\mathrm{m}},\omega_{\mathrm{R}}t]{} \mathrm{LF},\ \mathbf{B}_0. \quad [3]$$

In this case, the angular-dependent frequency depends on all three Euler angles (α, β, γ), on all elements of the chemical shift tensor in the MF (which is usually nondiagonal in this frame), as well as explicitly on time (*1*):

$$\begin{aligned}\omega(t) &= \omega(\alpha, \beta, \gamma + \omega_{\mathrm{R}}t)\\ &= C_1^{\mathrm{nd}}\cos(\gamma + \omega_{\mathrm{R}}t) + C_2^{\mathrm{nd}}\cos(2\gamma + 2\omega_{\mathrm{R}}t)\\ &\quad + S_1^{\mathrm{nd}}\sin(\gamma + \omega_{\mathrm{R}}t) + S_2^{\mathrm{nd}}\sin(2\gamma + 2\omega_{\mathrm{R}}t), \quad [4]\end{aligned}$$

where the isotropic part has been omitted from the equation and explicit expressions for the coefficients $C_1^{\mathrm{nd}}(\alpha, \beta, \underline{\underline{\sigma}}^{\mathrm{MF}})$, $C_2^{\mathrm{nd}}(\alpha, \beta, \underline{\underline{\sigma}}^{\mathrm{MF}})$, $S_1^{\mathrm{nd}}(\alpha, \beta, \underline{\underline{\sigma}}^{\mathrm{MF}})$, $S_2^{\mathrm{nd}}(\alpha, \beta, \underline{\underline{\sigma}}^{\mathrm{MF}})$ are given elsewhere (*1*, *22*, *23*). Note that the dependencies in Eq. [4] can always be written in terms of the sum of $(\gamma + \omega_{\mathrm{R}}t)$, because both γ and $\omega_{\mathrm{R}}t$ correspond to rotations about the rotor axis.

For a single segment, the MAS time-domain signal is then given by (*2*, *24*)

$$g(t) = \exp\left[i\int_0^t dt'\,\omega(t') \right]$$
$$= \exp(i\Phi(\alpha, \beta, \gamma + \omega_R t, \underline{\underline{\sigma}}^{MF}))\exp(-i\Phi(\alpha, \beta, \gamma, \underline{\underline{\sigma}}^{MF}))$$
$$= f^*(\alpha, \beta, \gamma, \underline{\underline{\sigma}}^{MF})\, f(\alpha, \beta, \gamma + \omega_R t, \underline{\underline{\sigma}}^{MF}), \quad [5]$$

where the so-called *f*-functions are given by (*2*)

$$f(\alpha, \beta, \gamma + \omega_R t, \underline{\underline{\sigma}}^{MF}) = \exp(i\Phi(\alpha, \beta, \gamma + \omega_R t, \underline{\underline{\sigma}}^{MF})). \quad [6]$$

Note that the *f*-functions are periodic with

$$f(\alpha, \beta, \gamma, \underline{\underline{\sigma}}) = f(\alpha, \beta, \gamma + n2\pi, \underline{\underline{\sigma}})$$
$$= f(\alpha, \beta, \gamma + n\omega_R T_R, \underline{\underline{\sigma}}) \quad [7]$$

for integer n; hence, all calculations can be confined to an interval of 2π. Sideband intensities are best calculated, as described by Mehring (*22*), by using the equalities

$$\exp(iz\sin\varphi) = \frac{1}{2\pi}\int_0^{2\pi} d\theta\ \delta(\theta - \varphi)\exp(iz\sin\theta), \quad \text{and}$$

$$\exp(iz\cos\varphi) = \frac{1}{2\pi}\int_0^{2\pi} d\theta\ \delta(\theta - \varphi)\exp(iz\cos\theta). \quad [8]$$

Letting $\varphi = \gamma + \omega_R t$ and inserting

$$1 = \frac{1}{2\pi}\int_0^{2\pi} d\theta\ \delta(\theta - \gamma - \omega_R t) \quad [9]$$

into Eq. [5], followed by expansion of the delta function into an infinite series of plane waves,

$$\delta(\theta - \gamma - \omega_R t) = \sum_{N=-\infty}^{\infty} \exp[-iN(\theta - \gamma - \omega_R t)], \quad [10]$$

yields the MAS time-domain signal:

$$g(t) = f^*(\alpha, \beta, \gamma, \underline{\underline{\sigma}}^{MF})$$
$$\times \frac{1}{2\pi}\int_0^{2\pi} d\theta\ \delta(\theta - \gamma - \omega_R t)\, f(\alpha, \beta, \theta, \underline{\underline{\sigma}}^{MF})$$
$$= \sum_{N=-\infty}^{\infty} e^{iN\omega_R t} e^{iN\gamma} f^*(\alpha, \beta, \gamma, \underline{\underline{\sigma}}^{MF})$$
$$\times \frac{1}{2\pi}\int_0^{2\pi} d\theta e^{-iN\theta} f(\alpha, \beta, \theta, \underline{\underline{\sigma}}^{MF})$$
$$= \sum_{N=-\infty}^{\infty} e^{iN\omega_R t} e^{iN\gamma} f^*(\alpha, \beta, \gamma, \underline{\underline{\sigma}}^{MF}) F_N(\alpha, \beta, \underline{\underline{\sigma}}^{MF}), \quad [11]$$

with $F_N(\alpha, \beta, \underline{\underline{\sigma}}^{MF})$ representing the Fourier transform of $f(\alpha, \beta, \theta, \underline{\underline{\sigma}}^{MF})$ with respect to θ (*1*):

$$F_N(\alpha, \beta, \underline{\underline{\sigma}}^{MF}) = \frac{1}{2\pi}\int_0^{2\pi} d\theta\ e^{-iN\theta} f(\alpha, \beta, \theta, \underline{\underline{\sigma}}^{MF}). \quad [12]$$

For a macroscopic sample, the contributions from all molecular orientations with different (α, β, γ) must be taken into account, weighted by the orientational distribution function $P(\alpha, \beta, \gamma)$, resulting in the signal for each species:

$$G(t) = \int_0^{2\pi} d\alpha \int_0^{\pi} \sin\beta\, d\beta \int_0^{2\pi} d\gamma\, P(\alpha, \beta, \gamma) e^{i\omega_{iso} t} g(t) h(t). \quad [13]$$

In Eq. [13] the evolution of the magnetization due to the isotropic chemical shift has been reintroduced, along with an appropriate apodization function $h(t)$ to take into account transverse relaxation with the time constant T_2, e.g., $h(t) = \exp(-t/T_2)$. A normalization constant for an isotropic powder sample $P(\alpha, \beta, \gamma) = \frac{1}{8\pi^2}$, has been used. The integration over γ then effectively produces a second FT with respect to γ, see Eq. [12], yielding the term $F_N^*(\alpha, \beta, \underline{\underline{\sigma}}^{MF})$ in Eq. [14]:

$$G(t) = \sum_{N=-\infty}^{\infty} e^{i\omega_{iso} t} e^{iN\omega_R t} \frac{1}{8\pi^2} \int_0^{2\pi} d\alpha \int_0^{\pi} \sin\beta d\beta$$
$$\times \int_0^{2\pi} d\gamma\, e^{iN\gamma} f^*(\alpha, \beta, \gamma, \underline{\underline{\sigma}}^{MF})\, F_N(\alpha, \beta, \underline{\underline{\sigma}}^{MF}) h(t)$$
$$= \sum_{N=-\infty}^{\infty} e^{i\omega_{iso} t} e^{iN\omega_R t} \frac{1}{4\pi} \int_0^{2\pi} d\alpha \int_0^{\pi} \sin\beta d\beta$$
$$\times F_N^*(\alpha, \beta, \underline{\underline{\sigma}}^{MF})\, F_N(\alpha, \beta, \underline{\underline{\sigma}}^{MF}) h(t)$$
$$= \sum_{N=-\infty}^{\infty} e^{i\omega_{iso} t} e^{iN\omega_R t} I_N^{MAS} h(t), \quad [14]$$

resulting in the positive and real values $F_N^*(\alpha, \beta, \underline{\underline{\sigma}}^{MF}) F_N(\alpha, \beta, \underline{\underline{\sigma}}^{MF}) = |F_N(\alpha, \beta, \underline{\underline{\sigma}}^{MF})|^2$, a property that is preserved during integration over α and β, producing positive sideband intensities I_N^{MAS} in the MAS spectrum (*25*). Fourier transformation of Eq. [14] yields a spectrum with peaks located at $\omega_N = \omega_{iso} + N\omega_R$, which have intensities given by $I_N^{MAS} = 1/4\pi \int_0^{2\pi} d\alpha \int_0^{\pi} \sin\beta d\beta F_N^* F_N$ and absorptive and dispersive lineshapes determined by $h(t)$:

$$I(\omega) = \sum_{N=-\infty}^{\infty} [A(\omega - \omega_N) + iD(\omega - \omega_N)] I_N^{MAS}. \quad [15]$$

Applying the TOSS pulse sequence (*13*), with four π-pulses applied at times τ_1 through τ_4 and signal acquisition starting at τ_5 after cross polarization, essentially suppresses the term $f^*(\alpha, \beta, \gamma, \underline{\underline{\sigma}}^{MF})$ in Eq. [5]. Thus, instead of Eq. [11], one obtains the time-domain signal:

$$g(t) = \sum_{N=-\infty}^{\infty} e^{iN\omega_R t} e^{iN\gamma} F_N(\alpha, \beta, \underline{\underline{\sigma}}^{MF}). \quad [16]$$

Integration over the angle γ then yields a delta function:

$$\begin{aligned} G(t) &= \sum_{N=-\infty}^{\infty} e^{i\omega_{iso} t} e^{iN\omega_R t} \frac{1}{8\pi^2} \int_0^{2\pi} d\alpha \int_0^{\pi} \sin\beta d\beta \\ &\quad \times \int_0^{2\pi} d\gamma\, e^{iN\gamma} F_N(\alpha, \beta, \underline{\underline{\sigma}}^{MF}) h(t) \\ &= \sum_{N=-\infty}^{\infty} e^{i\omega_{iso} t} e^{iN\omega_R t} \frac{1}{4\pi} \int_0^{2\pi} d\alpha \int_0^{\pi} \sin\beta d\beta \\ &\quad \times F_N(\alpha, \beta, \underline{\underline{\sigma}}^{MF}) \delta_{N,0} h(t) \\ &= \frac{1}{4\pi} \int_0^{2\pi} d\alpha \int_0^{\pi} \sin\beta d\beta\, F_0(\alpha, \beta, \underline{\underline{\sigma}}^{MF}) e^{i\omega_{iso} t} h(t) \\ &= I_0^{TOSS} e^{i\omega_{iso} t} h(t), \end{aligned} \quad [17]$$

with the result that a centerband-only spectrum is obtained, the intensity I_0^{TOSS} of which is in general different from the intensity I_0^{MAS} of the centerband in the conventional MAS spectrum (*26*).

Monitoring Random Jump Motions with EIS

In the EIS experiment shown in Fig. 1c, at the point τ_5 where the acquisition begins in a standard TOSS measurement, the transverse ^{13}C magnetization is rotated to the z-direction by a $\pi/2$-pulse, and a mixing time begins. The mixing period is allowed to last an integral number of rotor periods, during which frequency exchanges can occur that ultimately reintroduce spinning sidebands into the spectrum. At the end of the mixing period, the magnetization is returned to the transverse plane by another $\pi/2$-pulse for detection of the signal. Depending on the phase of the pulse at the beginning of the mixing period, either the sine or the cosine component of the transverse magnetization (or more precisely, the real or imaginary part of the complex time-domain signal, respectively) is selected for detection after the mixing period. Both components have to be measured and added to obtain the EIS spectrum. Although the summation of the two components can be achieved in a single experiment by using the appropriate pulse phases and adding the time-domain signals, it is preferable to obtain the sine and cosine components in separate experiments and combine the data afterwards, thereby preserving the possibility to adjust their respective phases independently. In the absence of frequency changes, for example due to molecular motions, the mixing period has no effect other than to allow spin–lattice relaxation to occur. Under these circumstances, the spectrum displays only centerband signals at the isotropic chemical shifts; the effect of magnetization created by spin–lattice relaxation is eliminated by proper phase cycling. In the presence of molecular motion (or magnetization transfer by spin diffusion), however, the delicate nonequilibrium state of the nuclear spins prepared by the TOSS sequence is perturbed during the mixing time, with the consequence that sidebands arise in the spectrum.

Before the mixing time, the signal of a single molecular segment is thus given by either the real or imaginary part of the complex TOSS signal, $f_1(\alpha, \beta, \gamma + \omega_R\tau_5, \underline{\underline{\sigma}}^{MF})$, depending on the phase of the pulse preceding t_m. After the mixing time, the signal evolves as a normal MAS free-induction decay (FID), resulting in the EIS time-domain signal for a single molecule or molecular segment:

$$\begin{aligned} g^{ij}_{Re,Im}(t; t_m) = {}& {}^{Re}_{Im}[f_1(\alpha, \beta, \gamma + \omega_R\tau_5, \underline{\underline{\sigma}}_i^{MF})] \\ & \times f_2^*(\alpha, \beta, \gamma + \omega_R\tau_5 + \omega_R t_m, \underline{\underline{\sigma}}_j^{MF}) \\ & \times f_2(\alpha, \beta, \gamma + \omega_R\tau_5 + \omega_R t_m + \omega_R t, \underline{\underline{\sigma}}_j^{MF}). \end{aligned} \quad [18]$$

The amplitude of the complex signal detected after the mixing time is proportional to the real or imaginary part of the signal prepared by the TOSS sequence before the mixing time. Thus, the resulting EIS time-domain signal for a particular set of Euler angles (α, β, γ) with respect to the rotor frame is a MAS FID, phase-shifted by $\omega_R t_m$ and multiplied by the real number $\mathrm{Re}[f_1(\alpha, \beta, \gamma, \underline{\underline{\sigma}}_i^{MF})]$ or $\mathrm{Im}[f_1(\alpha, \beta, \gamma, \underline{\underline{\sigma}}_i^{MF})]$. The subscripts 1 and 2 on the f-functions refer to the orientations associated with the chemical shift tensors relative to the mol-

ecule-fixed (MF) frame at the beginning and at the end of the mixing time, respectively. The indices $i, j = 1, \ldots, Z$ label the number of sites Z among which exchange takes place, and $\underline{\underline{\sigma}}_i^{\mathrm{MF}}$ or $\underline{\underline{\sigma}}_j^{\mathrm{MF}}$ represent the chemical shift tensors in site i or site j, respectively. For a particular molecular segment in the sample, the contribution to the EIS time-domain signal is

$$g(t;\, t_m) = \sum_{i,j}^{Z} P'_{ij}(t_m)[\, g^{ij}_{\mathrm{Re}}(t;\, t_m) + i g^{ij}_{\mathrm{Im}}(t;\, t_m)], \qquad [19]$$

with

$$\begin{aligned} P'_{ij}(t_m) &= [\exp(\underline{\underline{K}} t_m)]_{ji} P_i \\ &= [\exp((\underline{\underline{\Pi}} - \underline{\underline{R}}) t_m)]_{ji} P_i, \end{aligned} \qquad [20]$$

where $P_i = P(\underline{\underline{\sigma}}_i)$ is the equilibrium population of site i with chemical shift tensor $\underline{\underline{\sigma}}_i$, $\underline{\underline{\Pi}}$ is the exchange matrix with elements Π_{nm}, which for $m \neq n$ gives the probability per unit time for exchange from site m to site n, and $\underline{\underline{R}}$ is a diagonal matrix with elements $1/T_1^j$ that account for spin–lattice relaxation at the different sites. Assuming that the T_1 values are the same for all sites, Eq. [20] simplifies to

$$\begin{aligned} P'_{ij}(t_m) &= \exp\left(-\frac{t_m}{T_1}\right)[\exp(\underline{\underline{\Pi}} t_m)]_{ji} P_i \\ &= P_{ij}(t_m) \exp\left(-\frac{t_m}{T_1}\right), \end{aligned} \qquad [21]$$

where the joint probability density $P_{ij}(t_m) = P(\underline{\underline{\sigma}}_i, \underline{\underline{\sigma}}_j; t_m)$ is the fractional population of those nuclei that at the beginning of the mixing time were in site i with chemical shift tensor $\underline{\underline{\sigma}}_i$ and at its end are in site j with chemical shift tensor $\underline{\underline{\sigma}}_j$. Note that even in the absence of motion, the overall signal (Eq. [19]) decays with the relaxation time T_1.

The joint probability density $P_{ij}(t_m) = P(\underline{\underline{\sigma}}_i, \underline{\underline{\sigma}}_j; t_m)$ can be expressed as the product of the probability density $P_i = P(\underline{\underline{\sigma}}_i)$ of finding a molecule with chemical shift tensor $\underline{\underline{\sigma}}_i$ and the conditional probability density $W_{ji}(t_m) = W(\underline{\underline{\sigma}}_j; t_m | \underline{\underline{\sigma}}_i)$ that its tensor is $\underline{\underline{\sigma}}_j$ at time t_m, provided it was $\underline{\underline{\sigma}}_i$ before the mixing time. In that regard, the matrix $\underline{\underline{W}}$ consists of i column vectors $\mathbf{W}_i$, the j elements of which are recognized as the conditional probabilities $W(\underline{\underline{\sigma}}_j; t_m | \underline{\underline{\sigma}}_i)$ of finding a particle on site j at time t_m, if it was initially at site i at $t = 0$. For a stationary Markov process, the conditional probability density $W_{ji}(t_m)$ follows the set of differential equations

$$\frac{\partial}{\partial t} W_{ji}(t) = \sum_{k=1}^{Z} \Pi_{jk} W_{ki}(t), \qquad [22]$$

with the initial condition $W_{ji}\ (t = 0) = \delta_{ij}$. The simple case of jumps among Z equally populated equivalent sites ($P_j = 1/Z$), with the probability k_{hop} of a jump between any two sites is described by an exchange matrix whose elements are all k_{hop}, except for the diagonal terms, which are $-(Z-1)k_{\mathrm{hop}}$. Defining the microscopic rate coefficient k_{mic} as the overall rate for leaving a single site, $k_{\mathrm{mic}} = (Z-1)k_{\mathrm{hop}}$, yields the relation $\tau_c = P_j/k_{\mathrm{hop}} = 1/(Zk_{\mathrm{hop}}) = (Z-1)/(Zk_{\mathrm{mic}})$ between the correlation time τ_c and the various rate coefficients. The differential equations (Eq. [22]) can then be solved to obtain

$$\begin{aligned} W_{ji}(t_m) &= \frac{1}{Z} + \left(\delta_{ij} - \frac{1}{Z}\right)\exp(-Zk_{\mathrm{hop}} t_m) \\ &= \exp\left(-\frac{t_m}{\tau_c}\right)\delta_{ij} + \left[1 - \exp\left(-\frac{t_m}{\tau_c}\right)\right]\frac{1}{Z}, \end{aligned} \qquad [23]$$

or in terms of the joint probability density

$$\begin{aligned} P_{ij}(t_m) &= W_{ji}(t_m) P_i \\ &= \exp\left(-\frac{t_m}{\tau_c}\right)\delta_{ij} P_i + \left[1 - \exp\left(-\frac{t_m}{\tau_c}\right)\right] P_i P_j. \end{aligned} \qquad [24]$$

That means $P_{ij}(t_m)$ is simply a linear combination of $P_{ij}(t_m = 0) = \delta_{ij} P_i$ (no exchange) and $P_{ij}(t_m \to \infty) = P_i P_j$ (full exchange) for arbitrary values of t_m. This property is characteristic for models describing random jumps (all jump rates proportional to P_j) from an arbitrary orientation to any other orientation among equivalent sites or random jumps among inequivalent sites with a single common reorientation geometry.

Static 2D Exchange Orientational Autocorrelation Functions

Before proceeding with the analysis of the EIS experiment, the static 2D exchange NMR experiment will be discussed briefly, because it stands out among all of the one- and two-dimensional exchange NMR experiments in that the 2D exchange spectrum $S(\omega_1, \omega_2; t_m)$ represents a direct mapping of the joint probability density $P_{ij}(t_m)$ into the (ω_1, ω_2)-frequency space (*10*). Hence, from Eq. [24] it can be directly concluded that for random jump-type motions among equivalent sites, the associated static 2D exchange spectrum $S(\omega_1, \omega_2; t_m)$ is a linear combination of the diagonal spectrum and the spectrum for full exchange (*1, 10b*). For any type of reorientation dynamics and the special case of $\eta = 0$ (axially symmetric interaction tensor), only the Euler angle β between the z-principal axis of the coupling tensor and the external magnetic field is needed to describe the reorientation geometry. In these circumstances, calculating the two-time frequency average:

$$\begin{aligned} \langle \omega_1 \omega_2 \rangle(t_m) &= \langle \omega(0)\omega(t_m) \rangle \\ &= \int\int d\omega_1 d\omega_2 \omega_1 \omega_2 S(\omega_1, \omega_2; t_m) \end{aligned} \qquad [25]$$

is equivalent to calculating the second-order orientational autocorrelation function $C_2(t_m)$ (*1*):

$$C_2(t_m) = 5\langle P_2(\cos(\beta(t=0)))\, P_2(\cos(\beta(t=t_m)))\rangle = \frac{5}{\delta^2}\langle\omega(0)\omega(t_m)\rangle. \quad [26]$$

This provides direct and model-free access to the motional correlation time τ_c from a series of static 2D exchange NMR spectra that have been acquired as a function of the mixing time: The experimental spectral intensity $S(\omega_1, \omega_2; t_m)$ is integrated numerically, weighted by the product of the frequency coordinates of the individual points.

For $\eta = 0$, the 2D exchange spectra are uniquely determined by a one-dimensional reorientation angle distribution $R(\beta_3; t_m)$, where the reorientation angle $\beta_3 = \beta_2 - \beta_1$ is the angle between the relative orientations $\beta_1 = \beta\ (t = 0)$ and $\beta_2 = \beta(t = t_m)$, of the chemical shift tensor during t_1 and t_2, respectively (*1, 10*):

$$S(\omega_1, \omega_2; t_m) = \int_{0^\circ}^{90^\circ} d\beta_3\, R(\beta_3; t_m) S_{\beta_3}(\omega_1, \omega_2). \quad [27]$$

This integral represents the sum of the subspectra for each reorientation angle, $S_{\beta_3}(\omega_1, \omega_2)$, weighted by factors $R_f(\beta_3; t_m)$ for $0° \le \beta_3 \le 180°$. Because of the equivalence of the spectra for β_3 and $180° - \beta_3$, integration is restricted to $0° \le \beta_3 \le 90°$:

$$R(\beta_3; t_m) = R_f(\beta_3; t_m) + R_f(180° - \beta_3; t_m). \quad [28]$$

Thus, a relation equivalent to Eq. [26] is obtained by expressing the process in terms of the reorientational angle β_3 relative to the initial position $\beta_3\ (t = 0) = 0°$:

$$C_2(t_m) = \langle P_2(\cos(\beta_3\ (t=0) = 0°))\, P_2(\cos(\beta_3\ (t=t_m)))\rangle = \langle P_2(\cos(\beta_3(t_m)))\rangle = \int_{0^\circ}^{90^\circ} d\beta_3\, R(\beta_3; t_m)\, P_2(\cos(\beta_3(t_m))). \quad [29]$$

Equation [29] allows for straightforward calculation of the autocorrelation function $C_2(t_m)$ based solely on the reorientation angle distribution $R(\beta_3; t_m)$. For a random jump-type motion among equivalent sites, the reorientation angle distribution is given by

$$R(\beta_3; t_m) = \exp\left(-\frac{t_m}{\tau_c}\right)\delta(\beta_3) + \left[1 - \exp\left(-\frac{t_m}{\tau_c}\right)\right] R(\beta_3; t_m \to \infty), \quad [30]$$

which results in the expected monoexponential decay of the correlation function $C_2(t_m)$:

$$\begin{aligned} C_2(t_m) &= \int_{0^\circ}^{90^\circ} d\beta_3\, P_2(\cos(\beta_3(t_m)))\left[\exp\left(-\frac{t_m}{\tau_c}\right)\delta(\beta_3) + \left[1 - \exp\left(-\frac{t_m}{\tau_c}\right)\right] R\left(\beta_3; t_m \to \infty\right)\right] \\ &= \left[1 - \int_{0^\circ}^{90^\circ} d\beta_3\, R(\beta_3; t_m \to \infty)\, P_2(\cos(\beta_3(t_m)))\right] \\ &\quad \times \exp\left(-\frac{t_m}{\tau_c}\right) + \int_{0^\circ}^{90^\circ} d\beta_3\, R(\beta_3; t_m \to \infty)\, P_2(\cos(\beta_3(t_m))) \\ &= (1 - \lim_{t_m \to \infty} C_2(t_m; \beta_3))\exp\left(-\frac{t_m}{\tau_c}\right) + \lim_{t_m \to \infty} C_2(t_m; \beta_3). \end{aligned} \quad [31]$$

As indicated, in the limit of long mixing times, a plateau value $\lim_{t_m \to \infty} C_2(t_m; \beta_3)$ is reached, which depends on the reorientation angle β_3 and reorientation angle distribution $R(\beta_3; t_m)$. For example, for a random jump motion between four equivalent, equally populated, tetrahedrally arranged sites, $\lim_{t_m \to \infty} C_2(t_m; \beta_3) = 0.25{*}P_2(\cos(0°)) + 0.75{*}P_2(\cos(109.5°)) = 0$. This approach to calculating the orientational autocorrelation function from static 2D exchange spectra appears to be a general one. Its suitability has additionally been demonstrated for motional processes involving isotropic rotational diffusion, and also when nonaxially symmetric interaction tensors are present, in which case the normalization factor in Eq. [26] needs to be replaced by $(5/\delta^2)(1/(1 + \eta^2/3))$ (*1, 16*).

Comparison of MAS Exchange Experiments

Proceeding with the analysis of the EIS experiment, the mixing time is set to an integral number of rotor periods (otherwise sidebands will be present in the EIS spectrum even in the absence of dynamics.) Consequently, the term $\omega_R t_m$ can be omitted from Eq. [18] because of the periodicity of the *f*-functions, so that the EIS time-domain signal for a single molecule or molecular segment becomes

$$g(t;\, t_{\mathrm{m}}) = \sum_{i,j} P_{ij}(t_{\mathrm{m}})\exp\left(-\frac{t_{\mathrm{m}}}{T_1}\right) \times f_1(\alpha,\, \beta,\, \phi,\, \underline{\sigma}_i^{\mathrm{MF}})\, f_2^*(\alpha,\, \beta,\, \phi,\, \underline{\sigma}_j^{\mathrm{MF}}) \times f_2(\alpha,\, \beta,\, \phi + \omega_{\mathrm{R}}t,\, \underline{\sigma}_j^{\mathrm{MF}}), \quad [32]$$

where $\phi = \gamma + \omega_{\mathrm{R}}\tau_5$. From Eq. [32], the full EIS signal is obtained after integration over the three Euler angles α, β, and γ. Introducing again the evolution due to the isotropic chemical shift and damping function $h(t)$ yields the EIS time-domain signal, which can be compared with Eqs. [14] and [17] for the time-domain MAS and TOSS signals, respectively:

$$G(t;\, t_{\mathrm{m}}) = \frac{1}{8\pi^2}\int_0^{2\pi} d\alpha \int_0^{\pi} \sin\beta d\beta \int_0^{2\pi} d\gamma\, e^{i\omega_{\mathrm{iso}}t} g(t;\, t_{\mathrm{m}})h(t) = \sum_{N=-\infty}^{\infty} e^{i\omega_{\mathrm{iso}}t} e^{iN\omega_{\mathrm{R}}t} I_N^{\mathrm{EIS}}(t_{\mathrm{m}})h(t), \quad [33]$$

where $I_N^{\mathrm{EIS}}(t_{\mathrm{m}})$ is the intensity of the Nth-order sideband in the EIS spectrum, as given by

$$I_N^{\mathrm{EIS}}(t_{\mathrm{m}}) = \sum_{i,j} P_{ij}(t_{\mathrm{m}})\exp\left(-\frac{t_{\mathrm{m}}}{T_1}\right) I_N^{ij,\mathrm{EIS}} = \sum_{i,j} P_{ij}(t_{\mathrm{m}})\exp\left(-\frac{t_{\mathrm{m}}}{T_1}\right) \sum_{M=-\infty}^{\infty} e^{iM\omega_{\mathrm{R}}\tau_5} I_{MN}^{ij,\mathrm{EIS}}. \quad [34]$$

In Eq. [34] we applied the notation $I_N^{ij,\mathrm{EIS}}$ and $I_{MN}^{ij,\mathrm{EIS}}$ to facilitate comparison of the expressions for the intensities of the center- and sidebands in the EIS spectrum with those observed in rotor-synchronized MAS 2D exchange, ODESSA, and time-reverse ODESSA experiments, $I_{MN}^{ij,\mathrm{2D}}$, $I_N^{ij,\mathrm{ODESSA}}$ and $I_N^{ij,\mathrm{trODESSA}}$ used in Refs. (*2, 5, 8, 9*). For these measurements, the $I_{MN}^{ij,\mathrm{2D}}$ values represent the unweighted exchange cross peaks (or diagonal peaks if $i = j$) correlating the Mth Fourier component of site i with the Nth component of site j, and are given by the expression

$$I_{MN}^{ij,\mathrm{2D}} = \frac{1}{4\pi}\int_0^{2\pi} d\alpha \int_0^{\pi} d\beta \sin\beta\, (F_M^i)^* F_{M-N}^{i,j} F_N^j, \quad [35]$$

where

$$F_N^j = F_N(\alpha,\, \beta,\, \underline{\sigma}_j^{\mathrm{MF}}) = \frac{1}{2\pi}\int_0^{2\pi} d\xi\, e^{-iN\xi} f(\alpha,\, \beta,\, \xi,\, \underline{\sigma}_j^{\mathrm{MF}}) \quad [36]$$

$$F_{M-N}^{i,j} = F_{M-N}(\alpha,\, \beta,\, \underline{\sigma}_i^{\mathrm{MF}},\, \underline{\sigma}_j^{\mathrm{MF}}) = \frac{1}{2\pi}\int_0^{2\pi} d\xi\, e^{-i(M-N)\xi} f_1(\alpha,\, \beta,\, \xi,\, \underline{\sigma}_i^{\mathrm{MF}})\, f_2^*(\alpha,\, \beta,\, \xi,\, \underline{\sigma}_j^{\mathrm{MF}}). \quad [37]$$

Using Eq. [35], the intensites of the Nth-order sidebands in ODESSA or time-reverse ODESSA spectra are calculated as (*8, 9*):

$$I_N^{\mathrm{ODESSA}}(t_{\mathrm{m}}) = \sum_{i,j} P_{ij}(t_{\mathrm{m}})\exp\left(-\frac{t_{\mathrm{m}}}{T_1}\right) I_N^{ij,\mathrm{ODESSA}}, \quad [38]$$

where

$$I_N^{ij,\mathrm{ODESSA}} = \sum_{M=-\infty}^{\infty} (-1)^M I_{MN}^{ij,\mathrm{2D}} \quad [39]$$

$$I_N^{ij,\mathrm{trODESSA}} = \sum_{M=-\infty}^{\infty} (-1)^M (-1)^N I_{MN}^{ij,\mathrm{2D}}. \quad [40]$$

Applying the same notation to describe the unweighted intensity of the Nth-order sideband in the EIS spectrum, the corresponding expressions for $I_{MN}^{ij,\mathrm{EIS}}$ and $I_N^{ij,\mathrm{EIS}}$ in Eq. [34] become

$$I_{MN}^{ij,\mathrm{EIS}} = \frac{1}{4\pi}\int_0^{2\pi} d\alpha \int_0^{\pi} d\beta \sin\beta\, \delta_{M,0} F_{M-N}^{i,j} F_N^i, \quad [41]$$

and

$$I_N^{ij,\mathrm{EIS}} = \sum_{M=-\infty}^{\infty} e^{iM\omega_{\mathrm{R}}\tau_5} \frac{1}{4\pi}\int_0^{2\pi} d\alpha \int_0^{\pi} \sin\beta d\beta\, \delta_{M,0} F_{M-N}^{i,j} F_N^j = \frac{1}{4\pi}\int_0^{2\pi} d\alpha \int_0^{\pi} \sin\beta d\beta\, F_{0-N}^{i,j} F_N^j. \quad [42]$$

Equations [41] and [42] contain a delta function $\delta_{M,0}$ as opposed to $(F_M^i)^*$ (Eq. [35]) because of the TOSS sequence in EIS, analogous to the difference between Eqs. [14] and [17].

From Eq. [42], it can be seen that the phase factor $e^{iM\omega_{\mathrm{R}}\tau_5}$, which appears in Eq. [34] multiplying the sideband intensities $I_{MN}^{ij,\mathrm{EIS}}$ and which could lead to severe phase distortions in the resulting spectrum, actually has no effect; the delta function in the integral for $I_{MN}^{ij,\mathrm{EIS}}$, Eq. [41], causes the phase to factor vanish altogether with the sum over M. This results from the application of the TOSS sequence before the mixing time to suppress all of the sidebands. More precisely, the cancellation

of the phase factor is a consequence of the Hahn-echo condition of the TOSS sequence, which causes the signal to be refocused at time τ_5 (*1*). The Hahn-echo condition is also responsible for the beneficial circumstance that the occurrence of different isotropic chemical shifts, and consequently more than one family of spinning sidebands in the EIS spectrum, does not result in phase-distorted spectra, as is observed in the ODESSA experiment (*9*). There, for a spin system consisting of several distinct groups of equivalent nuclei with different isotropic chemical shifts $\omega^a_{\rm iso}$, $\omega^b_{\rm iso}$, . . . , the ODESSA time-domain signal becomes

$$G^{\rm ODESSA}(t;\, t_{\rm m}) = \sum_a \exp\left(i\omega^a_{\rm iso}\frac{T_{\rm R}}{2}\right) \times \sum_{N=-\infty}^{\infty} \exp(i(\omega^a_{\rm iso} + N\omega_{\rm R})t) I_N^{a,{\rm ODESSA}}(t_{\rm m}), \quad [43]$$

where Σ_a reflects summation over the different species present. It is clear from Eq. [43] that each sideband family is associated with different phase factors $\omega^a_{\rm iso}\, T_{\rm R}/2$. The EIS signal by comparison is free of this difficulty, again as a result of the Hahn-echo condition inherent to the TOSS pulse sequence:

$$G^{\rm EIS}(t;\, t_{\rm m}) = \sum_a \sum_{N=-\infty}^{\infty} \exp(i(\omega^a_{\rm iso} + N\omega_{\rm R})t) I_N^{a,{\rm EIS}}(t_{\rm m}). \quad [44]$$

The phase difficulties of the ODESSA experiment can, however, be overcome by performing time-reverse ODESSA (*9*), which cancels distortions arising from the preceding phase factors; see Eq. [43]. Phase distortions, however, can still occur in the time-reverse ODESSA experiment, if the dynamic process involves exchange between groups with different isotropic shifts, resulting in "phase transfer" (*9*):

$$G^{\rm trODESSA}(t;\, t_{\rm m}) = \sum_b \sum_{N=-\infty}^{\infty} (-1)^N \exp(i(\omega^b_{\rm iso} + N\omega_{\rm R})t) \times \sum_{ai}\sum_j P_{aibj}(t_{\rm m}) \exp\left(i(\omega^b_{\rm iso} - \omega^a_{\rm iso})\frac{T_{\rm R}}{2}\right) I_N^{aibj}, \quad [45]$$

where the NMR interaction tensors before the mixing time are labeled with the single index ai, and the sum over the tensors after the mixing time indexed by bj has been separated into sums over the isotropic b and anisotropic j parts. When exchange occurs between different groups, phase factors $(\omega^b_{\rm iso} - \omega^a_{\rm iso})T_{\rm R}/2$ appear, leading to phase distortions. While such phase distortions in time-reverse ODESSA spectra complicate analysis of the data, they can nevertheless be used to separate multiple dynamic processes, such as molecular reorientation and magnetization transfer via spin diffusion (*9*). Again, due to the Hahn-echo condition of the TOSS sequence, such phase distortions do not exist in EIS spectra, even for the case of chemical exchange between groups with different isotropic chemical shifts.

Additionally, differences are apparent between the EIS experiment and MAS 2D, ODESSA, or time-reverse ODESSA measurements, based on a comparison of Eqs. [35] and [41]. In the expression for $I^{ij,{\rm EIS}}_{MN}$ in Eq. [41], a delta function replaces the $(F^i_M)^*$ term in Eq. [35], indicating that different sideband intensities are expected for the different experiments. To demonstrate this, Fig. 3 compares the center- and sideband intensities of simulated EIS (Fig. 3(a)) and time-reverse ODESSA spectra (Fig. 3(b)) (which are identical to the intensities of the ODESSA spectra), as functions of the reorientation angle β_3 for the case of a two-site exchange process involving an axially symmetric chemical shift tensor in the limit of full exchange ($t_{\rm m} \rightarrow \infty$). The intensities of the centerbands and first- and second-order sidebands are shown in Fig. 3 for a spinning speed of $\omega_{\rm R} = 2\pi \times 0.4\ \delta$ (see Eq. [1]), which was selected as a compromise between rapid spinning with little or no sideband intensity and very slow spinning with low or negative TOSS intensity (*13c, 24, 26*). Specifically, the relative intensities of EIS and time-reverse ODESSA sidebands are functions of both reorientation geometry and sample spinning speed (in addition to chemical shift tensor values). The intensity of the EIS centerband in Fig. 3a decreases with increasing reorientation angle, while the EIS sidebands generally increase in intensity as β_3 becomes larger. In contrast, the intensities of all time-reverse ODESSA peaks in Fig. 3b decrease with increasing β_3 at low reorientation angles. The intensity of the time-reverse ODESSA centerband in Fig. 3b decreases over the entire range of reorientation angles from 0° to 90°, while the intensity curves of some sidebands increase slightly at higher reorientation angles. For example, the intensity of the $N = -2$ time-reverse ODESSA sideband I_{-2} decreases with increasing reorientation angle from 0° to about 35°, then steadily increases at higher jump angles up to 90°. Intensity changes in an Nth-order time-reverse ODESSA (or ODESSA) peak as a function of reorientation angle β_3 reflect variations in the corresponding MAS 2D exchange peak intensities $I^{ij,{\rm 2D}}_{MN}$ summed over M, for $M - N$ even compared to $M - N$ odd; see Eqs. [35] through [40].

Focusing on the relative intensity variations of the sidebands of the EIS and time-reverse ODESSA spectra, the plots in Fig. 3 reflect a significant dependence on reorientation angle β_3. For small reorientation angles, the EIS sidebands show less overall change in their intensities relative to the EIS spectrum obtained in the absence of motion, compared to the respective time-reverse ODESSA spectra. For example, a reorientation angle of 20° leads to reductions of both time-reverse ODESSA and EIS *centerbands* by about 8% compared to the total re-

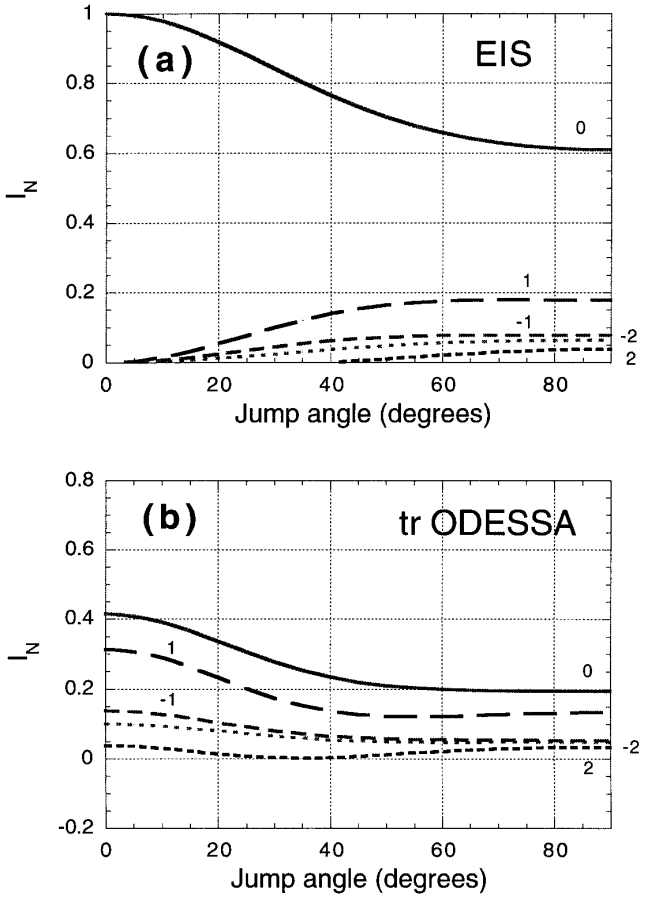

FIG. 3. Simulated center- (I_0) and sideband (I_N, $N \neq 0$) peak intensities for an axially symmetric chemical shift tensor undergoing a slow two-site jump motion through a variable jump angle, β_3, while the sample is spinning at $\omega_R = 2\pi \times 0.4\delta$. Peak orders N for each of the curves are indicated on the graphs. Peak intensities are normalized to the no-motion ($\beta_3 = 0°$) limit. (a) The EIS centerband decays, while the EIS sidebands generally rise with increasing reorientation angle, so that the sum over all EIS peak intensities remains constant. The changes in peak intensities with changing reorientation angle are stronger in the center of the curves (20° to 60°) and weaker at the edges, near 0° and 90°. (b) Time-reverse ODESSA peak intensities, which are the same for the ODESSA experiment. Note that the dependencies of the peak intensities on the jump angles are more pronounced over the range 0° to 50° and relatively weak from 50° to 90°.

spective spectral intensities measured by the two experiments in the absence of such reorientation dynamics. However, the collective intensity changes of the time-reverse ODESSA *sidebands* are approximately twice those of the EIS sidebands. While the EIS sidebands rise to a combined intensity of about 8% of the no-exchange EIS spectrum for a reorientation angle of 20°, such motion yields a decrease in the combined intensities of the time-reverse ODESSA sidebands by about 16%. In contrast, for reorientation angles from about 65° to 90°, the increase in intensity summed over all EIS sidebands is slightly larger than the corresponding decrease in intensity summed over all time-reverse ODESSA sidebands. These differences show the EIS experiment under these conditions to be less sensitive to small reorientation angles and of similar sensitivity at large (>65°) reorientation angles compared to MAS 2D exchange or ODESSA.

In the absence of exchange, the shift tensors $\underline{\underline{\sigma}}_i$ and $\underline{\underline{\sigma}}_j$ in Eq. [37] are identical, and the f-functions cancel in the integral ($f^*f = 1$). Performing the integration in Eq. [37] then results in $F^{i,j}_{M-N} = \delta_{M,N}$, so that the sideband intensities in Eq. [35] are equal to the intensities in the conventional MAS experiment (Eq. [14]):

$$I^{2D}_{M,N} = \frac{1}{4\pi}\int_0^{2\pi} d\alpha \int_0^{\pi} d\beta \sin\beta\, F^*\delta_{M,N}F_N = \delta_{M,N}I^{MAS}_N. \qquad [46]$$

Analogously, for the EIS spectrum in the absence of exchange, Eq. [41] becomes

$$I^{EIS}_N = \frac{1}{4\pi}\int_0^{2\pi} d\alpha \int_0^{\pi} d\beta \sin\beta\,\delta_{N,0}F_0 = \delta_{N,0}I^{TOSS}_0 \qquad [47]$$

and a centerband-only spectrum is observed (Eq. [17]).

Combining Eqs. [24], [34], [42], and [47] yields the expression for the intensities of the sidebands in an EIS spectrum for the case of random jump motions among Z equivalent sites:

$$\begin{aligned} I^{EIS}_N(t_m) &= \sum_{i,j}\left[\exp\left(-\frac{t_m}{\tau_c}\right)\delta_{ij}P_i \right. \\ &\quad \left. + \left[1-\exp\left(-\frac{t_m}{\tau_c}\right)\right]P_iP_j\right]\exp\left(-\frac{t_m}{T_1}\right)I^{ij,EIS}_N \\ &= \exp\left(-\frac{t_m}{T_1}\right)\left[\sum_{i,j}\exp\left(-\frac{t_m}{\tau_c}\right)\delta_{ij}P_iI^{ij,EIS}_N \right. \\ &\quad \left. + \sum_{i,j}\left[1-\exp\left(-\frac{t_m}{\tau_c}\right)\right]P_iP_jI^{ij,EIS}_N\right] \\ &= \exp\left(-\frac{t_m}{T_1}\right)\left[\delta_{N,0}I^{TOSS}_0\exp\left(-\frac{t_m}{\tau_c}\right) \right. \\ &\quad \left. + \left[1-\exp\left(-\frac{t_m}{\tau_c}\right)\right]I^{fe,EIS}_N\right], \end{aligned} \qquad [48]$$

with:

$$I^{fe,EIS}_N = \sum_{ij} P_iP_jI^{ij,EIS}_N, \qquad [49]$$

from which the final absorptive EIS spectrum $I^{EIS}(\omega)$ can be computed as $I^{EIS}(\omega) = \Sigma^{\infty}_{N=-\infty} A(\omega - \omega_N)I^{EIS}_N$ (analogous to taking the real part of Eq. [15].)

Extraction of Correlation Times

Equation [48] represents the EIS spectrum for random jump-type motions as being composed of the sum of the no-exchange TOSS spectrum, which decays as $\exp(-t_m/\tau_c)$, and the full-exchange spectrum $I_N^{fe,EIS}$, which rises to its final value as $\exp(-t_m/\tau_c)$, analogous to the case of the static 2D exchange NMR experiment discussed earlier. Therefore, taking the ratio $R^{EIS}(t_m)$ of the combined intensities of all sidebands (excluding the centerband) and the integrated intensity of the entire spectrum eliminates the exponential factor associated with the T_1 relaxation. This allows the motional correlation time τ_c to be determined directly from a series of EIS spectra that have been acquired as a function of the mixing time, without the need for explicit determination of T_1:

$$R^{EIS}(t_m) = \frac{\sum_{N\neq 0} I_N^{EIS}(t_m)}{\sum_N I_N^{EIS}(t_m)} = \frac{\sum_{N\neq 0}\left[1-\exp\left(-\frac{t_m}{\tau_c}\right)\right] I_N^{fe,EIS}}{\left[I_0^{TOSS}\exp\left(-\frac{t_m}{\tau_c}\right)+\sum_N\left[1-\exp\left(-\frac{t_m}{\tau_c}\right)\right] I_N^{fe,EIS}\right]}. \quad [50]$$

To proceed, the sum over all peaks in the full exchange EIS spectrum I_N^{fe} needs to be evaluated. Using Eqs. [36], [37], [42], [47], [49] and the relation $\sum_{N=-\infty}^{\infty}\exp(iN(\theta-\varphi)) = \delta(\theta-\varphi)$ (analogous to Eq. [10]), one arrives at

$$\begin{aligned}\sum_N I_N^{fe,EIS} &= \sum_N\sum_{i,j} P_iP_j\, I_N^{ij,EIS}\\ &= \sum_N\sum_{i,j} P_iP_j\,\frac{1}{4\pi}\int_0^{2\pi} d\alpha\int_0^{\pi}\sin\beta d\beta\; F_{0-N}^{i,j}F_N^j\\ &= \sum_{i,j} P_iP_j\,\frac{1}{4\pi}\int_0^{2\pi} d\alpha\int_0^{\pi}\sin\beta d\beta\,\frac{1}{4\pi^2}\\ &\quad\times\int_0^{2\pi} d\varphi\int_0^{2\pi} d\theta\;\delta(\theta-\varphi)\, f_1(\alpha,\beta,\theta,\underline{\sigma}_i^{MF})\\ &\quad\times f_2^*(\alpha,\beta,\theta,\underline{\sigma}_j^{MF})\, f_2(\alpha,\beta,\varphi,\underline{\sigma}_j^{MF})\\ &= \sum_{i,j} P_iP_j\,\frac{1}{4\pi}\int_0^{2\pi} d\alpha\int_0^{\pi}\sin\beta d\beta\; F_0\\ &= \sum_{i,j} P_iP_j I_0^{TOSS} = I_0^{TOSS}, \end{aligned} \quad [51]$$

so that Eq. [50] can be rewritten as

$$R^{EIS}(t_m) = \frac{\sum_{N\neq 0} I_N^{fe,EIS}}{I_0^{TOSS}}\left[1-\exp\left(-\frac{t_m}{\tau_c}\right)\right] = R^{fe}\left[1-\exp\left(-\frac{t_m}{\tau_c}\right)\right], \quad [52]$$

where the abbreviation R^{fe} denotes the sum over all sidebands intensities (excluding the centerband) in the full-exchange (fe) limit ($t_m\to\infty$), normalized with respect to the centerband-only TOSS spectrum intensity.

Equation [52] is very similar to the expression obtained for the ratio of the combined intensities of the off-diagonal cross-peaks to the total integrated area of all peaks in the rotor-synchronized MAS 2D exchange NMR experiment $R^{2D,MAS}(t_m)$. Analogous to Eq. [48], the intensities of the MAS 2D exchange peaks are given by

$$\begin{aligned} I_{MN}^{2D}(t_m) &= \sum_{i,j} P_{ij}(t_m)\exp\left(-\frac{t_m}{T_1}\right) I_{MN}^{ij,2D}\\ &= \exp\left(-\frac{t_m}{T_1}\right)\left[\delta_{M,N} I_N^{MAS}\exp\left(-\frac{t_m}{\tau_c}\right)\right.\\ &\quad\left.+\left[1-\exp\left(-\frac{t_m}{\tau_c}\right)\right] I_{MN}^{fe,2D}\right], \end{aligned} \quad [53]$$

where Eqs. [24] and [46] have been used and with

$$I_{MN}^{fe,2D} = \sum_{i,j} P_iP_j I_{MN}^{ij,2D}; \quad [54]$$

$I_{MN}^{ij,2D}$ is given by Eq. [35]. The rotor-synchronized MAS 2D exchange spectrum for random jump-type motions is the sum of a no-exchange MAS spectrum (Eq. [46]) which decays as $\exp(-t_m/\tau_c)$, and the full-exchange spectrum (Eq. [54]) which rises to its final value as $\exp(-t_m/\tau_c)$, yielding for the ratio of the intensity of off-diagonal cross peaks to total spectral intensity:

$$R^{2D,MAS}(t_m) = \frac{\sum_M\sum_{N\neq M} I_{MN}^{fe,2D}}{\sum_N I_N^{MAS}}\left[1-\exp\left(-\frac{t_m}{\tau_c}\right)\right]. \quad [55]$$

Similarly, for the case of the static (non-spinning) 2D exchange experiment:

$$R^{2D}(t_m) = \sum_i\sum_{j\neq i} P_iP_j\left[1-\exp\left(-\frac{t_m}{\tau_c}\right)\right]. \quad [56]$$

In contrast to Eq. [55] for the 2D MAS exchange experiment, where the prefactor is comprised of a combination of the site populations and the sideband intensities, Eq. [56] for the static 2D

exchange experiment in general yields direct information about the number of sites Z involved in the random jump motion, provided symmetry does not render some of the sites equivalent.[3] Executing the double sum in Eq. [56] for equally populated sites yields

$$R^{2D}(t_m) = \frac{Z-1}{Z}\left[1 - \exp\left(-\frac{t_m}{\tau_c}\right)\right]. \qquad [57]$$

For a random jump motion among equivalent sites, ODESSA spectra are also composed of the sum of a no-exchange spectrum and a full-exchange spectrum (Eqs. [24], [38]). ODESSA spectra contain positive and negative peaks, so summing over the intensities of all ODESSA sidebands or the entire spectrum involves adding large positive and negative numbers to obtain a small value. Consequently, the ratio of the combined ODESSA sideband intensities to the total ODESSA spectrum intensity (analogous to the analysis of EIS spectra using $R^{EIS}(t_m)$ in Eq. [50]) may be sensitive to small experimental imperfections, such as noise, associated with implementation of the ODESSA experiment. Alternatively, taking the ratio of the integrated area of one peak to the total spectral intensity yields greater sensitivity to reorientation and still permits the extraction of a motional correlation time τ_c without explicitly determining T_1. For convenience, taking the negative value of the integral intensity when an odd-numbered sideband appears in the numerator yields a ratio that decreases monotonically with increasing mixing time:

$$R_N^{ODESSA}(t_m) = \frac{(-1)^N I_N^{ODESSA}(t_m)}{\sum_N I_N^{ODESSA}(t_m)} = \frac{e^{t_m/\tau_c} I_N^{MAS} + [1 - e^{t_m/\tau_c}]\sum_M (-1)^M (-1)^N I_{MN}^{fe,2D}}{e^{t_m/\tau_c}\sum_N (-1)^N I_N^{MAS} + [1 - e^{t_m/\tau_c}]\sum_N \sum_M (-1)^M I_{MN}^{fe,2D}}, \qquad [58]$$

where Eqs. [24], [38], [39], [46], and [54] have been used. The double-summation term containing $I_{MN}^{fe,2D}$ in the denominator may be further simplified, because the sums over M and N are equivalent. The sum over the intensities of the peaks along a given column or row in the 2D exchange spectrum is constant (neglecting a T_1 relaxation factor in both the numerator and denominator of Eq. [58], which cancels), independent of t_m, and equals the intensity of the corresponding sideband in the 1D MAS spectrum:

$$\sum_N I_{MN}^{fe,2D} = \sum_M I_{MN}^{fe,2D} = I_{M \text{ or } N}^{MAS}, \qquad [59]$$

[3] For example, because of the inversion center of a benzene molecule, NMR frequency changes due to the six-site jump motion in the plane of the molecule are indistinguishable from frequency changes due to a three-site jump motion.

with the result that

$$R_N^{ODESSA}(t_m) = \frac{e^{t_m/\tau_c} I_N^{MAS} + [1 - e^{t_m/\tau_c}]\sum_M (-1)^M (-1)^N I_{MN}^{fe,2D}}{e^{t_m/\tau_c}\sum_N (-1)^N I_N^{MAS} + [1 - e^{t_m/\tau_c}]\sum_M (-1)^M I_M^{MAS}} = \frac{\sum_M (-1)^M (-1)^N I_{MN}^{fe,2D} + (I_N^{MAS} - \sum_M (-1)^M (-1)^N I_{MN}^{fe,2D}) e^{t_m/\tau_c}}{\sum_N (-1)^N I_N^{MAS}}. \qquad [60]$$

Using a direct analogy for the time-reverse ODESSA analysis, i.e., taking the ratio of one peak to the entire spectrum, also eliminates the need to determine or fit T_1 explicitly. This ratio is similar to, but not the same as, Eq. [58]:

$$\frac{I_N^{trODESSA}(t_m)}{\sum_N I_N^{trODESSA}(t_m)} = \frac{e^{t_m/\tau_c} I_N^{MAS} + [1 - e^{t_m/\tau_c}]\sum_M (-1)^M (-1)^N I_{MN}^{fe,2D}}{e^{t_m/\tau_c}\sum_N I_N^{MAS} + [1 - e^{t_m/\tau_c}]\sum_M \sum_N (-1)^M (-1)^N I_{MN}^{fe,2D}}. \qquad [61]$$

However, the ratio in Eq. [61] will not be used here for analysis of time-reverse ODESSA spectra, because the double-summation term in the denominator cannot be simplified using Eq. [59], due to the appearance of both $(-1)^N$ and $(-1)^M$ in the sums containing the $I_{MN}^{fe,2D}$ term.

An expression equivalent to Eq. [58], however, may be obtained for time-reverse ODESSA spectra by modifying the intensity ratio from that used in Eq. [61]. ODESSA and time-reverse ODESSA signals are closely related (see Eqs. [39], [40]), and, in the absence of phase distortion, a time-reverse ODESSA spectrum can be converted into an ODESSA spectrum by inverting all of the odd-numbered sidebands. Doing so permits the same simplification (Eq. [59]) used to obtain Eq. [60], thereby allowing the motional correlation time to be more conveniently extracted from a series of time-reverse ODESSA spectra:

$$R_N^{trODESSA}(t_m) = \frac{I_N^{trODESSA}(t_m)}{\sum_N (-1)^N I_N^{trODESSA}(t_m)} = \frac{e^{t_m/\tau_c} I_N^{MAS} + [1 - e^{t_m/\tau_c}]\sum_M (-1)^M (-1)^N I_{MN}^{fe,2D}}{e^{t_m/\tau_c}\sum_N (-1)^N I_N^{MAS} + [1 - e^{t_m/\tau_c}]\sum_M (-1)^M (-1)^{2N} I_{MN}^{fe,2D}} = \frac{\sum_M (-1)^M (-1)^N I_{MN}^{fe,2D} + (I_N^{MAS} - \sum_M (-1)^M (-1)^N I_{MN}^{fe,2D}) e^{t_m/\tau_c}}{\sum_N (-1)^N I_N^{MAS}}. \qquad [62]$$

Equation [62] has a simpler form and fewer parameters than Eq. [61], making it more convenient to use in the analysis.

While a correlation time τ_c may be extracted directly from a series of static 2D exchange, MAS 2D exchange, EIS, ODESSA, or time-reverse ODESSA NMR spectra (Eqs. [57], [55], [52], [60], and [62], respectively) there are important differences among these experiments. The ratios for 2D exchange and EIS spectra contain two fitting parameters, namely a correlation time and a full-exchange limit, but only the full-exchange limit of the static 2D exchange ratio $R^{2D}(t_m)$ yields directly the number of sites Z participating in the exchange process. While it is the most experimentally time-consuming of the experiments discussed here, static 2D exchange NMR also gives direct access to the orientational autocorrelation function $C_2(t_m)$, which permits extraction of a correlation time for types of molecular reorientational motion other than random jumps. Unlike EIS spectra, ODESSA or time-reverse ODESSA spectra obtained in the absence of molecular reorientation contain sidebands: The spectra are MAS spectra with every odd-numbered sideband either inverted (ODESSA) or not (time-reverse ODESSA). Consequently, because $R_N^{\mathrm{ODESSA}}(t_m = 0) = R_N^{\mathrm{trODESSA}}(t_m = 0) \neq 0$, fitting the ratios for ODESSA and time-reverse ODESSA spectra requires three fitting parameters, one of which may be obtained from MAS peak intensities. The ODESSA and time-reverse ratios also each contain a sum over $(-1)^N I_N^{\mathrm{MAS}}$ in their denominators, which involves adding positive and negative peaks to obtain a small value. Thus, the errors for correlation times obtained from ODESSA and time-reverse ODESSA are expected to be larger than for correlation times determined on the basis of EIS spectra. For the conditions considered here ($\eta = 0$, $\omega_R = 2\pi \times 0.4\delta$), the EIS experiment is less sensitive to small reorientation angles than the ODESSA, time-reverse ODESSA, or MAS 2D exchange experiments, although at large reorientation angles ($>65°$) the sensitivities are similar. Finally, when multiple isotropic shifts are present in the spectra, peaks in ODESSA spectra are phase-distorted. The phases of peaks in time-reverse ODESSA spectra are distorted if isotropic shifts change during the mixing time, while EIS and MAS 2D exchange are free of this difficulty. All of these exchange NMR experiments quantify the same correlation time τ_c, and consistency among the exchange NMR experiments may be checked by conducting several of these experiments on the same sample, as will be shown later.

RESULTS AND DISCUSSION

The relationship among the EIS, ODESSA, time-reverse ODESSA, and static 2D exchange NMR techniques can be clearly seen by examining slow dynamic processes in solid, polycrystalline dimethylsulfone (DMS), $(CH_3)_2SO_2$. The simple, well-studied molecular reorientation dynamics of DMS make it an excellent compound for comparing the measurements and analyses of motional correlation times obtained using the different exchange NMR methods. The use of DMS with ^{13}C in natural abundance (1.1%) renders magnetization transfer via spin diffusion inefficient; thus, molecular motions are the sole source(s) of NMR frequency changes giving rise to exchange features in the ^{13}C NMR spectra. Furthermore, these results can be compared against literature values for DMS exchange rates determined using other ^{13}C and ^{2}H NMR measurement strategies (*27–29*).

In a crystal, DMS molecules undergo slow twofold π-flips about their individual C_2 symmetry axes, which exchange the positions of each pair of otherwise chemically equivalent methyl groups. The reorientation angles for the z-axes of the ^{13}C chemical shift and ^{2}H electric field gradient tensors associated with the methyl groups are close to the angles between two vertices of a tetrahedron ($\beta_3 = 109.5°$). The elliptical ridges of a static 2D exchange ^{13}C NMR spectrum and simulations of static ^{13}C lineshapes yield a value of 108° for the reorientation angle, while the elliptical ridges and a best-fit reconstruction of selected ω_1 slices of a 2D exchange ^{2}H NMR spectrum yield 106° and 108°, respectively (*27, 30*). Additionally, ^{13}C VACSY experiments (*31*) and 2D exchange ^{2}H NMR in the intermediate exchange regime (*32*) have been performed on DMS, using kinetic parameters based on the Arrhenius equations reported in Refs. *27* and *33*.

Figure 4 shows experimental ODESSA, time-reverse ODESSA, TOSS, and EIS ^{13}C NMR spectra acquired on DMS spinning at $\omega_R = 2\pi \times 1800$ Hz and at $T = 289$ K. For ODESSA and time-reverse ODESSA the primary effect of dynamics is an overall decay of the entire spectrum with increasing mixing time, diminished further by T_1 relaxation; slight changes in ODESSA and time-reverse ODESSA relative peak intensities are a subtle secondary effect. As shown in Fig. 4a, top, the ODESSA spectrum acquired with a mixing time of approximately 3 ms closely resembles the spectrum (Fig. 2a, top) simulated for the case of no exchange. ODESSA spectra acquired with mixing times of approximately 16 and 50 ms (Fig. 4a, middle and bottom) show diminished intensity, consistent with the simulated spectra in Fig. 2a, middle and bottom. The time-reverse ODESSA spectra, shown in Fig. 4b and acquired with the same parameters as the spectra in Fig. 4a, also show decreasing intensity with increasing mixing time, consistent with the simulations in Fig. 2b. Slight differences in some relative peak intensities between the experimental and simulated time-reverse ODESSA spectra in Figs. 4b and 2b are attributed to their sensitive dependence on the cross-polarization parameters employed.[4] The sideband intensities of the experimental EIS spectra in Fig. 4c rise with increasing mixing time, while the centerband intensity decreases. The

[4] Relative peak intensities are sensitive to the cross-polarization (CP) parameters; for example, a time-reverse ODESSA spectrum acquired with a CP contact time of 4 ms (not shown) instead of 2 ms (Fig. 4b, top) was virtually identical to the simulated spectrum in Fig. 2b, top. All spectra in Fig. 4 were obtained using identical CP parameters.

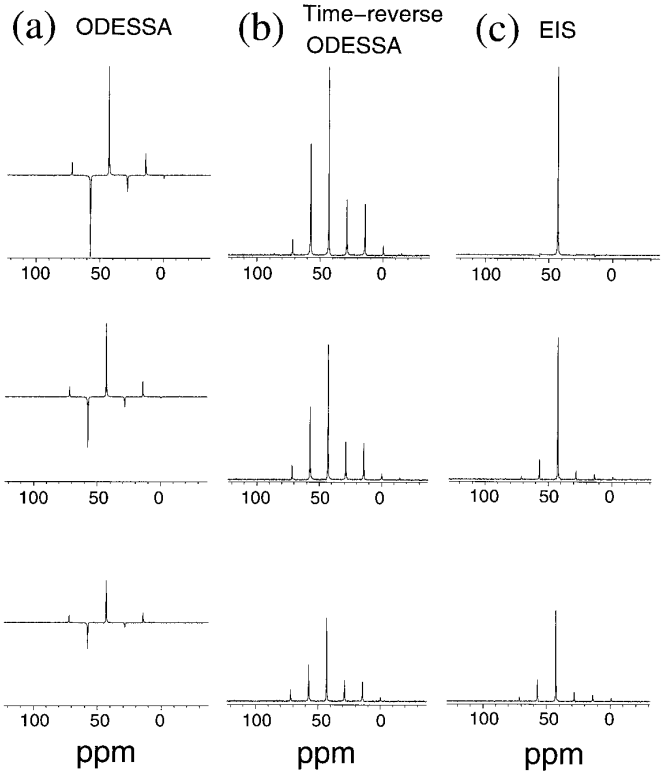

FIG. 4. Experimental ^{13}C NMR of spectra of DMS obtained using different solid-state exchange NMR techniques while spinning at $\omega_R = 2\pi \times 1800$ Hz at a temperature of $T = 289$ K. (a) ODESSA spectra with mixing times of approximately 3, 16, and 50 ms. (b) Time-reverse ODESSA spectra with mixing times of approximately 3, 16, and 50 ms. (c) TOSS spectrum and EIS spectra with mixing times of approximately 16 and 50 ms. The dominant effect of dynamics for ODESSA and time-reverse ODESSA spectra is a reduction in the intensity of the entire spectrum with increasing mixing time, whereas for the EIS spectra it is the reappearance of spinning sidebands.

experimental EIS spectra in Fig. 4c show excellent agreement with the EIS simulations in Fig. 2c.

If the time scale for molecular reorientation and the T_1 relaxation time are widely separated (by a factor of about 10 or greater), both may be extracted simultaneously from a biexponential fit to the intensity of a single ODESSA peak as a function of mixing time. The centerband intensity $I_0^{\mathrm{ODESSA}}(t_m)$ and $N = 1$ sideband intensity $I_1^{\mathrm{ODESSA}}(t_m)$, for example, typically show significant decreases with increasing mixing time. Such biexponential fits to ODESSA and time-reverse ODESSA peaks have been used to quantify molecular reorientation rates $k = 1/(2\tau_c)$ in DMS (*8, 9*). Rates of $k = 65.2$ s^{-1} ($\tau_c = 8$ ms) and 112 s^{-1} ($\tau_c = 4$ ms) at $T = 298$ and 305 K, respectively, have been reported using ODESSA and $k = 71$ s^{-1} ($\tau_c = 7$ ms) at $T = 298$ K using time-reverse ODESSA; discrepancies were found between the fit T_1 values and those obtained from independent measurements, and the reason for the discrepancies is not yet known (*8, 9*). At slightly lower temperatures the T_1 relaxation and motional time scales are similar. In this case, time scales for molecular reorientations may be obtained after applying T_1 corrections from independent measurements, or the data may be analyzed according to the ratios $R_N^{\mathrm{ODESSA}}(t_m)$ in Eq. [58] or $R_N^{\mathrm{trODESSA}}(t_m)$ in Eq. [62], which do not require explicit determination of T_1.

Figure 5a shows that the centerband ratio $R_0^{\mathrm{ODESSA}}(t_m)$ (filled symbols) and sideband ratio $R_1^{\mathrm{ODESSA}}(t_m)$ (open symbols) for ODESSA spectra obtained on DMS at $T = 289$ K both decrease with increasing mixing time. The lines are fits to $a^*\exp(-t_m/\tau_c) + b$, which yield correlation times of $\tau_c = 17 \pm 6$ ms and 18 ± 6 ms, reflecting self-consistent agreement between two different peaks in the same series of ODESSA spectra. The corresponding time-reverse ODESSA ratios (Eq. [62]) obtained from a series of spectra for DMS at $T = 289$ K are shown in Fig. 5b. The fits to $a^*\exp(-t_m/\tau_c) + b$ in Fig. 5b are similar to Fig. 5a, although not identical; nevertheless, the correlation times $\tau_c = 19 \pm 7$ ms and 20 ± 7 ms obtained from the time-reverse ODESSA results in Fig. 5b agree with the ODESSA measurements within the experimental uncertainties.

The correlation times for dimethylsulfone measured at $T = 289$ K are also in good agreement with the EIS and static 2D exchange data shown in Figs. 5c and 5d, respectively. As the EIS sidebands increase with increasing mixing time, the EIS ratio $R^{\mathrm{EIS}}(t_m)$ (Fig. 5c) rises with increasing t_m. The EIS data are fit to $c^*(1 - \exp(-t_m/\tau_c))$ (Eq. [52]), which contains one less fitting parameter than the fits to the ODESSA and time-reverse ODESSA results in Figs. 5a and 5b (R^{EIS} $(t_m = 0) = 0$). Because changes in relative peak intensities are the dominant effect of dynamics in the EIS spectra, rather than a secondary effect as in the ODESSA spectra, the fit in Fig. 5c yields a correlation time with higher precision, $\tau_c = 16 \pm 2$ ms. The EIS full-exchange limit of $c = R^{\mathrm{fe}} = 0.34 \pm 0.01$ comprises a combination of site populations and sideband intensities (see Eqs. [49], [50]), which are influenced by chemical shift tensor values and spinning speed, as well as reorientation angles (see Eqs. [32]–[34]). This is in contrast to the 2D exchange data, which yield site populations and geometric information directly. The ratio of off-diagonal to total intensity $R^{\mathrm{2D}}(t_m)$ of a single slice in the 2D spectrum, shown by the open symbols in Fig. 5d, yields a full-exchange limit of 0.50 ± 0.04, a model-independent verification of a two-site jump process (Eq. [57]). This is consistent with twofold π-flips that exchange the positions of the methyl groups in $(CH_3)_2SO_2$. A fit to $d^*(1 - \exp(-t_m/\tau_c))$ yields a correlation time of $\tau_c = 21 \pm 4$ ms. Integration over the entire 2D spectrum to obtain the orientational autocorrelation function $C_2(t_m)$ (Eqs. [25], [26]), shown by the filled symbols in Fig. 5d, better utilizes the information present in the spectrum. A fit to $(1 - e)^*\exp(-t_m/\tau_c) + e$ (Eq. [31]) yields a correlation time of $\tau_c = 19 \pm 2$ ms. Taking the ^{13}C chemical shift tensor of DMS ($\eta \approx 0.08$) to be axially symmetric, the full-exchange limit of $C_2(t_m)$ in Fig. 5d is 0.32 ± 0.02, consistent with a 108° jump angle, $0.5^*P_2(\cos(0°)) + 0.5^*P_2(\cos(108°)) = 0.32$. Results obtained at other temperatures show similar consistency among

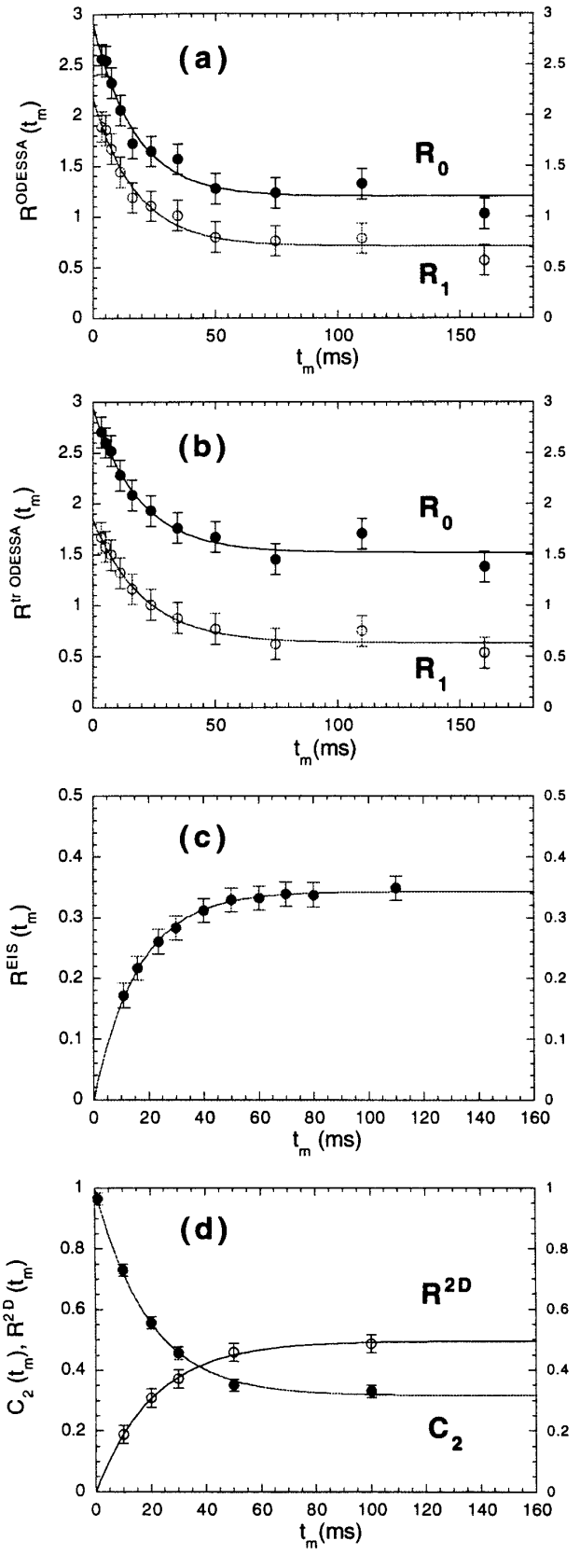

TABLE 1

Motional Correlation Times τ_c for Dimethylsulfone (DMS) over the Temperature Range 271 to 289 K, as Determined from the Different Exchange ^{13}C NMR Experiments Indicated

Temperature (K)	EIS τ_c (ms)	ODESSA τ_c (ms)	Time-reverse ODESSA τ_c (ms)	2D exchange τ_c (ms)
271	125 ± 16	134 ± 47	132 ± 46	—
275	92 ± 12	105 ± 37	115 ± 40	114 ± 17
280	53 ± 7	49 ± 17	64 ± 22	—
284	29 ± 4	40 ± 14	37 ± 13	40 ± 6
289	16 ± 2	17 ± 6	20 ± 7	20 ± 3

measurements made using the different exchange NMR techniques.

Correlation times from EIS, ODESSA, time-reverse ODESSA, and static 2D exchange ^{13}C NMR measurements in the temperature range of $T = 271$ to 289 K are tabulated in Table 1. The ODESSA and time-reverse ODESSA correlation times reported are averages from the centerbands and $N = 1$ sidebands, and the 2D exchange correlation times are averages of $R^{2D}(t_m)$ and $C_2(t_m)$. Although there is some scatter, the correlation times generally agree within the estimated uncertainties. The DMS reorientation rate of $k = 29 \pm 19\ s^{-1}$ ($\tau_c = 17$ ms) measured at $T = 288$ K using on-resonance ^{2}H selective inversion-recovery (*29*) is also consistent with the correlation times measured at $T = 289$ K listed in Table 1; other values reported in Ref. (*29*) were obtained at higher temperatures. Decay of the exchange NMR signals due to short T_1 relaxation times prevents accurate quantification of the DMS reorientation time scale at temperatures significantly below 271 K using the exchange methods. Static 2D exchange ^{13}C NMR results were obtained at only three different temperatures because of the increased measuring time requirements of this experiment compared to the 1D MAS exchange methods.

FIG. 5. Extraction of motional correlation times from experimental DMS exchange ^{13}C NMR data at $T = 289$ K. (a) The ratios of ODESSA centerband intensities and $N = 1$ sideband intensities to the total intensity of the spectra, $R_0^{ODESSA}(t_m)$, filled symbols, and $R_1^{ODESSA}(t_m)$, open symbols, respectively, Eq. [58]. Corresponding fits to the data points are shown using a*exp($-t_m/\tau_c$) + b, which for the centerband ratio yields $a = 1.7 \pm 0.2$, $b = 1.2 \pm 0.1$, and $\tau_c = 17 \pm 6$ ms and for the sideband ratio $a = 1.4 \pm 0.2$, $b = 0.7 \pm 0.1$, and $\tau_c = 18 \pm 6$ ms. (b) The corresponding ratios for time-reverse ODESSA centerband intensities and $N = 1$ sideband intensities, $R_0^{trODESSA}(t_m)$, filled symbols, and $R_1^{trODESSA}(t_m)$, open symbols, respectively, Eq. [62]. The data have been fit using a*exp($-t_m/\tau_c$) + b, yielding $a = 1.4 \pm 0.2$, $b = 1.5 \pm 0.1$, and $\tau_c = 19 \pm 7$ ms for the centerband ratio and $a = 1.2 \pm 0.2$, $b = 0.6 \pm 0.1$, and $\tau_c = 20 \pm 7$ ms for the sideband ratio. (c) The ratio $R^{EIS}(t_m)$ of the EIS sideband intensities to total intensity, which has been fit using c*(1 − exp($-t_m/\tau_c$)), yielding $c = 0.34 \pm 0.01$ and $\tau_c = 16 \pm 2$ ms. (d) The ratio $R^{2D}(t_m)$ of static 2D exchange off-diagonal-to-total intensity (open symbols) for one slice of the spectrum where exchange and diagonal peaks are well separated and resolved. The data have been fit using d*(1 − exp($-t_m/\tau_c$)), yielding $d = 0.50 \pm 0.04$ and $\tau_c = 21 \pm 4$ ms. The orientational autocorrelation function $C_2(t_m)$ (filled symbols) is also shown and has been fit using (1 − e)*exp($-t_m/\tau_c$) + e, yielding $e = 0.32 \pm 0.02$ and $\tau_c = 19 \pm 2$ ms.

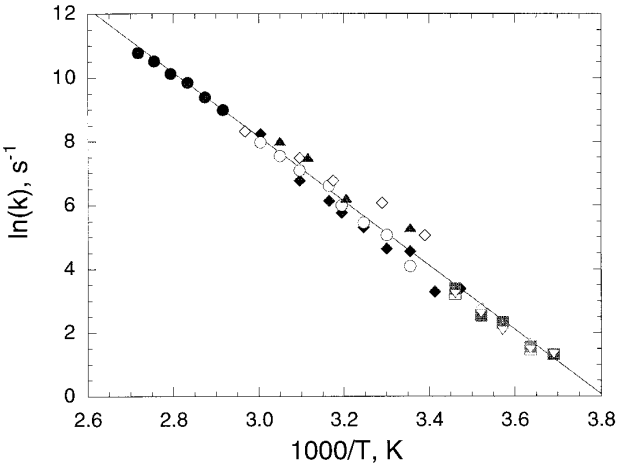

FIG. 6. Arrhenius plot of DMS reorientation rates as measured using a variety of ^{2}H and ^{13}C NMR techniques, including ^{2}H selective inversion on-resonance (filled diamonds) (*29*), ^{2}H selective inversion off-resonance (open circles) (*29*), ^{2}H static lineshape (filled circles) (*29*), ^{13}C static lineshape (open diamonds) (*27*), ^{13}C MAS (filled triangles) (*28*), ^{13}C EIS (open triangles), ^{13}C ODESSA (filled squares), ^{13}C time-reverse ODESSA (open inverted triangles), and 2D exchange ^{13}C NMR (open squares). To permit direct comparison, the rates from Ref. (*27*) have been divided by 2 and the exchange correlation times converted to rates using $k = 1/(2\tau_c)$. A single Arrhenius fit to all data yields $k_0 = 4 \times 10^{16}$ s^{-1} $\pm \frac{1}{2}$ decade and $E_a = 83 \pm 3$ kJ/mol.

The correlation times reported in Table 1 have been converted to rates $k = 1/(2\tau_c)$ for direct comparison to literature values obtained at higher temperatures, which are compiled in the Arrhenius plot in Fig. 6. A single fit to all data, spanning an approximately 100-K temperature range from 271 K to 368 K and spanning four orders of magnitude in the rate coefficients, yields an Arrhenius prefactor of $k_0 = 4 \times 10^{16}$ s^{-1} $\pm \frac{1}{2}$ decade and an apparent activation energy of $E_a = 83 \pm 3$ kJ/mol. At this scale, the rate coefficients measured using EIS, ODESSA, time-reverse ODESSA, and static 2D exchange ^{13}C NMR from $T = 271$ to 289 K overlap so tightly that it is difficult to distinguish their individual data points in the lower right-hand corner of the plot, a sign of their excellent agreement. Simulated 2D exchange ^{2}H NMR spectra obtained using this new set of kinetic parameters are in good agreement with the data of Kaufmann *et al.* (*32*). Brown *et al.* (*29*) have rationalized the large magnitude of the apparent preexponential factor by using a model in which k_0 was taken to be independent of temperature and a linearly temperature-dependent activation energy term was included. However, they also indicated that any weak temperature dependencies in the apparent Arrhenius parameters may lead to significant errors when extrapolating far from the data, with which we concur. Regardless, the reorientation jump rates for slow molecular reorientation in DMS, as measured by a variety of ^{13}C and ^{2}H NMR strategies, show excellent agreement over four orders of magnitude. Moreover, the rates determined from the EIS, ODESSA, time-reverse ODESSA, and static 2D ^{13}C exchange NMR measurements over the temperature range $T = 271$ to 289 K (Fig. 6, lower right corner) show greater consistency and less scatter compared to the rest of the data set.

CONCLUSIONS

In the study of slow molecular reorientation, static 2D exchange NMR gives information on the geometry and time scale of the motion directly and model-free. Quantification of the time scale, however, requires a series of spectra with varying mixing times, which is experimentally time-consuming, often prohibitively so. Measuring time requirements for characterizing random jump-type motions can be significantly reduced by using 1D MAS exchange techniques, namely EIS, ODESSA, or time-reverse ODESSA, which still permit the direct extraction of a correlation time without the need for explicit information on T_1 relaxation. ODESSA is suitable for samples in which only a single isotropic chemical shift is observed, while time-reverse ODESSA may be used on samples with multiple species yielding more than one isotropic shift; however, if exchange occurs between different isotropic shifts, then phase distortion of the time-reverse ODESSA spectrum will result. The EIS experiment is more flexible in this regard and yields generally more precise quantitative timescale measurements for large angle motions. However, sideband suppression using TOSS can be experimentally demanding, and EIS appears to be less sensitive than ODESSA or time-reverse ODESSA to small angle motions.

Molecular reorientational rates in DMS obtained using EIS, ODESSA, time-reverse ODESSA, and static 2D exchange ^{13}C NMR are shown to be consistent among the various exchange experiments over the temperature range of $T = 271$ to 289 K, as well as with other NMR techniques applicable to faster reorientation rates at higher temperatures. In addition, the direct extraction of motional correlation times using EIS has been recently demonstrated for benzene adsorbed on Ca-LSX zeolite (*18*). It appears that these approaches may be beneficial for extending the utility of the ODESSA and time-reverse ODESSA experiments into the regime where motional correlation times are on the order of T_1. The direct quantification of slow ($\tau_c = 10^{-3}$ to 10^1 s) molecular reorientation dynamics is relevant to a more thorough understanding of the properties of a wide variety of solids, including polymers, crystals of small organic molecules, and adsorbed molecules in nanoporous zeolites.

EXPERIMENTAL

EIS, ODESSA, and time-reverse ODESSA ^{13}C NMR spectra of DMS were measured on a Chemagnetics CMX-500 spectrometer operating at a ^{13}C frequency of 125.4 MHz and a ^{1}H frequency of 498.6 MHz. The sample was spun at $\omega_R = 2\pi \times 1800$ Hz in a 7.5-mm outer diameter zirconia PENCIL rotor. Long-term stability of better than ± 5 Hz was achieved using a Chemagnetics automatic spinning speed controller. For each of the foregoing

experiments, spectra were acquired at temperatures of $T = 271$, 275, 280, 284, and 289 K. The temperature was calibrated with methanol (*34*) and controlled using a standard variable temperature unit from Chemagnetics, with the accuracy, stability, and reproducibility estimated to be ± 1 K.

During the preparation period of the EIS experiment (Fig. 1c), a TOSS pulse sequence was used, with timings $\tau_1/T_R = 0.8111$, $\tau_2/T_R = 1.7699$, $\tau_3/T_R = 2.1888$, $\tau_4/T_R = 3.2301$, and $\tau_5/T_R = 4.0$ (*35*). Suppression of the sharp, narrow sidebands in a DMS spectrum with TOSS is experimentally demanding (*36*), and phase cycling of the TOSS sequence was essential to achieving effective sideband suppression (*1, 37*). The ^{13}C $\pi/2$ pulse length varied between 5.2 and 5.5 μs; a CP contact time of 2 ms and a recycle delay of 1 s were used. For each of the 1D MAS exchange experiments, two signals, which differed only in the phase of the pulse preceding the mixing time, were added to obtain the final spectrum. A total of 128 scans of 1024 complex points with a dwell time of 50 μs were collected for both the real and imaginary signals, resulting in a measuring time of about 4 min per spectrum. ODESSA and time-reverse ODESSA spectra were collected with mixing times t_m of approximately 3, 5, 7, 11, 16, 24, 34, 50, 74, 110, and 160 ms, while EIS spectra were collected at mixing times of approximately $t_m = 5$, 11, 16, 24, 30, 40, 50, 60, 70, 80, 110, and 160 ms.[5]

Static (nonspinning) 2D exchange ^{13}C NMR spectra were measured in off-resonance mode on a Chemagnetics CMX-500 spectrometer, at temperatures of 275, 284, and 289 K. A ^{13}C $\pi/2$ pulse length of 5.5 μs, CP contact time of 2 ms, a recycle delay of 1 s, and a delay between the two pulses of the Hahn echo of 60 μs were used for the static experiments. In the detection period, 128 complex points with a dwell time of 18 μs were acquired; 45 to 50 points in 36-μs increments were used for the evolution period. Prior to Fourier transformation, the data array was zero-filled to dimensions $(\omega_1 \times \omega_2) = 256 \times 512$. The final spectrum, with a spectral width of $2\pi \times 13.9$ kHz in both dimensions, was obtained by cutting the 2D array to dimensions 128×128 and discarding the $\frac{7}{8}$ of the 2D Fourier transform that contains either only baseline (ω_2) or the completely equivalent spectrum in the ω_1 dimension. Static 2D exchange spectra were measured at mixing times of $t_m = 1$, 10, 20, 30, 50, and 100 ms, as well as 120 ms at the lower temperatures; typical measuring times for one spectrum ranged from 2 to 6 h.

ACKNOWLEDGMENTS

The authors thank Professor K. Schmidt-Rohr, Professor Z. Luz, and Dr. D. Reichert for valuable discussions. Support from the U.S. National Science Foundation under the Young Investigator program (DMR-9257064), using instrumentation and facilities supported by the NSF Division of Materials Research under Grant DMR-9222527, and through the UCSB Materials Research Laboratory program under Award DMR-9632716 is gratefully acknowledged. Partial support has also been provided by Shell B. V., the David and Lucile Packard Foundation, and the U.S. Army Research Office (DAAH04-96-1-0443). B.F.C. is a Camille and Henry Dreyfus Teacher–Scholar and an Alfred P. Sloan Research Fellow.

[5] Due to technical details of the rotor synchronization, mixing times can be between $\frac{1}{2} T_R$ and $\frac{3}{2} T_R$ longer than reported; this uncertainty is not important to the data analysis.

REFERENCES

1. K. Schmidt-Rohr and H. W. Spiess, "Multidimensional Solid-State NMR and Polymers," Academic Press, San Diego (1994).
2. A. Hagemeyer, K. Schmidt-Rohr, and H. W. Spiess, Two-dimensional nuclear magnetic resonance experiments for studying molecular order and dynamics in static and in rotating solids, *Adv. Magn. Reson.* **13,** 85–130 (1989).
3. (*a*) A. F. de Jong, A. P. M. Kentgens, and W. S. Veeman, Two-dimensional exchange NMR in rotating solids: A technique to study very slow molecular reorientations, *Chem. Phys. Lett.* **109,** 337–342 (1984); (*b*) A. P. M. Kentgens, A. F. de Jong, E. de Boer, and W. S. Veeman, A 2D-exchange NMR study of very slow molecular motions in crystalline poly(oxymethylene), **18,** *Macromolecules,* 1045–1048 (1985); (*c*) A. P. M. Kentgens, E. de Boer, and W. S. Veeman, Ultraslow molecular motions in crystalline polyoxymethylene. A complete elucidation using two-dimensional solid state NMR, *J. Chem. Phys.* **87,** 6859–6866 (1987).
4. B. F. Chmelka, K. Schmidt-Rohr, and H. W. Spiess, Molecular dynamics in polymers studied by multidimensional solid-state NMR, *in* "Nuclear Magnetic Resonance Probes of Molecular Dynamics" (R. Tycko, Ed.), pp. 113–153, Kluwer Academic Publishers, Boston (1994).
5. Z. Luz, H. W. Spiess, and J. J. Titman, Rotor synchronized MAS two-dimensional exchange NMR in solids. Principles and applications, *Isr. J. Chem.* **32,** 145–160 (1992).
6. Y. Yang, M. Schuster, B. Blümich, and H. W. Spiess, Dynamic magic-angle spinning NMR spectroscopy: Exchange-induced sidebands, *Chem. Phys. Lett.* **139,** 239–243 (1987).
7. (*a*) S. Vega, Dynamic magic angle spinning NMR spectroscopy, *in* "Nuclear Magnetic Resonance Probes of Molecular Dynamics" (R. Tycko, Ed.), pp. 155–222, Kluwer Academic Publishers, Boston (1994); (*b*) Y. Yang, A. Hagemeyer, B. Blümich, and H. W. Spiess, 2D magic angle spinning NMR spectroscopy: Correlation between molecular order and dynamics, *Chem. Phys. Lett.* **150,** 1–5 (1988); (*c*) Y. Yang, A. Hagemeyer, and H. W. Spiess, Order-exchange correlated two-dimensional NMR study of slow molecular motion in highly oriented crystalline poly(oxymethylene), *Macromolecules* **22,** 1004–1006 (1989).
8. V. Gérardy-Montouillout, C. Malveau, P. Tekely, Z. Olender, and Z. Luz, ODESSA, a new 1D NMR exchange experiment for chemically equivalent nuclei in rotating solids, *J. Magn. Reson., Ser. A* **123,** 7–15 (1996).
9. D. Reichert, H. Zimmermann, P. Tekely, R. Poupko, and Z. Luz, Time-reverse ODESSA. A 1D exchange experiment for rotating solids with several groups of equivalent nuclei, *J. Magn. Reson.* **125,** 245–258 (1997).
10. (*a*) S. Wefing and H. W. Spiess, Two-dimensional exchange NMR of powder samples. I. Two-time distribution functions, *J. Chem. Phys.* **89,** 1219–1233 (1988); (*b*) S. Wefing, S. Kaufmann, and H. W. Spiess, Two-dimensional exchange NMR of powder samples. II. The dynamic evolution of two-time distribution functions, *J. Chem. Phys.* **89,** 1234–1244 (1988).
11. N. M. Szeverenyi, M. J. Sullivan, and G. E. Maciel, Observation of spin

exchange by two-dimensional Fourier transform ^{13}C cross polarization-magic-angle spinning, *J. Magn. Reson.* **47,** 462–475 (1982).

12. K. Zemke, K. Schmidt-Rohr, and H. W. Spiess, Polymer conformational structure and dynamics at the glass transition studied by multidimensional ^{13}C NMR, *Acta Polymerica* **45,** 148–159 (1994).

13. (*a*) W. T. Dixon, Spinning-sideband-free NMR spectra, *J. Magn. Reson.* **44,** 220–223 (1981); (*b*) W. T. Dixon, Spinning-sideband-free and spinning-sideband-only NMR spectra in spinning samples, *J. Chem. Phys.* **77,** 1800–1809 (1982); (*c*) D. P. Raleigh, E. T. Olejniczak, and R. G. Griffin, Multiple-pulse NMR in inhomogeneously broadened rotating solids: Theory of sideband suppression experiments, *J. Chem. Phys.* **89,** 1333–1350 (1988); (*d*) D. P. Raleigh, E. T. Olejniczak, S. Vega, and R. G. Griffin, An analysis of sideband suppression techniques in magic-angle sample spinning NMR, *J. Magn. Reson.* **72,** 238–250 (1987).

14. H. Geen and G. Bodenhausen, Pure absorption-mode chemical exchange nuclear magnetic resonance spectroscopy with suppression of spinning sidebands in a slowly rotating solid, *J. Chem. Phys.* **97,** 2928–2937 (1992).

15. G. S. Harbison, D. P. Raleigh, J. Herzfeld, and R. G. Griffin, High-field 2D exchange spectroscopy in rotating solids, *J. Magn. Reson.* **64,** 284–295 (1985).

16. G. A. Barrall, K. Schmidt-Rohr, Y. K. Lee, K. Landfester, H. Zimmermann, G. C. Chingas, and A. Pines, Rotational diffusion measurements of suspended colloidal particles using two-dimensional exchange nuclear magnetic resonance, *J. Chem. Phys.* **104,** 509–520 (1996).

17. (*a*) F. Fujara, S. Wefing, and H. W. Spiess, Dynamics of molecular reorientations: Analogies between quasielastic neutron scattering and deuteron NMR spin alignment, *J. Chem. Phys.* **84,** 4579–4584 (1986); (*b*) F. Fujara, S. Wefing, and W. F. Kuhs, Direct observation of tetrahedral hydrogen jumps in ice Ih, *J. Chem. Phys.* **88,** 6801–6809 (1988); (*c*) G. Fleischer and F. Fujara, NMR as a generalized incoherent scattering experiment, *in* "NMR Basic Principles and Progress," Vol. **30** (P. Diehl, E. Fluck, H. Günther, R. Kosfeld, J. Seelig, and B. Blümich, Eds.), pp. 159–207, Springer-Verlag, Berlin (1994).

18. D. J. Schaefer, D. E. Favre, M. Wilhelm, S. J. Weigel, and B. F. Chmelka, Site-hopping dynamics of benzene adsorbed on Ca-LSX zeolite studied by solid-state exchange ^{13}C NMR, *J. Am. Chem. Soc.* **119,** 9252–9267 (1997).

19. (*a*) D. Theimer and G. Bodenhausen, Selective inversion in inhomogeneously broadened powder spectra, *Appl. Magn. Reson.* **3,** 1071–1077 (1992); (*b*) D. Theimer and G. Bodenhausen, Shaped pulses for selective inversion of magnetization in solids spinning at the magic angle, *Appl. Magn. Reson.* **3,** 981–998 (1992).

20. J. Hong and G. S. Harbison, Magic-angle spinning sideband elimination by temporary interruption of the chemical shift, *J. Magn. Reson., Ser. A* **105,** 128–136 (1993).

21. (*a*) R. Challoner, J. Kümmerlen, and C. A. McDowell, Spectral spin diffusion under $\eta = 0$ rotational resonance, *Molecular Physics* **83,** 687–700 (1994); (*b*) J. Kümmerlen, J. D. van Beek, F. Vollrath, and B. H. Meier, Local structure in spider dragline silk investigated by two-dimensional spin-diffusion nuclear magnetic resonance, *Macromolecules* **29,** 2920–2928 (1996).

22. M. Mehring, "Principles of High-Resolution NMR in Solids," 2nd ed., Springer-Verlag, Berlin (1983).

23. (*a*) M. M. Maricq and J. S. Waugh, NMR in rotating solids, *J. Chem. Phys.* **70,** 3300–3316 (1979); (*b*) J. Herzfeld and A. E. Berger, Sideband intensities in NMR spectra of samples spinning at the magic angle, *J. Chem. Phys.* **73,** 6021–6030 (1980); (*c*) G. S. Harbison, V.-D. Vogt, and H. W. Spiess, Structure and order in partially oriented solids: Characterization by 2D-magic-angle-spinning NMR, *J. Chem. Phys.* **86,** 1206–1218 (1987).

24. E. T. Olejniczak, S. Vega, and R. G. Griffin, Multiple pulse NMR in rotating solids, *J. Chem. Phys.* **81,** 4804–4817 (1984).

25. M. H. Levitt, Why do spinning sidebands have the same phase? *J. Magn. Reson.* **82,** 427–433 (1989).

26. C. M. Rienstra, S. Vega, and R. G. Griffin, Centerband intensity in sideband-suppressed magic-angle-spinning spectra, *J. Magn. Reson., Ser. A* **119,** 256–259 (1996).

27. M. S. Solum, K. W. Zilm, J. Michl, and D. M. Grant, Carbon-13 line shape study of two-site exchange in solid dimethyl sulfone, *J. Phys. Chem.* **87,** 2940–2944 (1983).

28. A. Schmidt, S. O. Smith, D. P. Raleigh, J. E. Roberts, R. G. Griffin, and S. Vega, Chemical exchange effects in the NMR spectra of rotating solids, *J. Chem. Phys.* **85,** 4248–4253 (1986).

29. M. J. Brown, R. L. Vold, and G. L. Hoatson, Selective inversion investigations of slow molecular motion in solid state deuteron NMR spectroscopy, *Solid State NMR* **6,** 167–185 (1996).

30. (*a*) C. Schmidt, B. Blümich, and H. W. Spiess, Deuteron two-dimensional exchange NMR in solids, *J. Magn. Reson.* **79,** 269–290 (1988); (*b*) A. Hagemeyer, L. Brombacher, K. Schmidt-Rohr, and H. W. Spiess, Reconstruction of angular distributions from two-dimensional NMR spectra of powder samples, *Chem. Phys. Lett.* **167,** 583–587 (1990).

31. L. Frydman, S. Vallabhaneni, Y. K. Lee, and L. Emsley, Solid-state dynamic processes in complex systems analyzed by two-dimensional isotropic-anisotropic correlation nuclear magnetic resonance, *J. Chem. Phys.* **101,** 111–117 (1994).

32. S. Kaufmann, S. Wefing, D. Schaefer, and H. W. Spiess, Two-dimensional exchange nuclear magnetic resonance of powder samples. III. Transition to motional averaging and application to the glass transition, *J. Chem. Phys.* **93,** 197–214 (1990).

33. K. Schmidt-Rohr [personal communication].

34. A. L. Van Greet, Calibration of methanol nuclear magnetic resonance thermometer at low temperature, *Anal. Chem.* **42,** 679–680 (1970).

35. (*a*) S. J. Lang, Analytical expressions for TOSS sequences, *J. Magn. Reson., Ser. A* **104,** 345–346 (1993); (*b*) O. N. Antzutkin, Z. Song, X. Feng, and M. H. Levitt, Suppression of sidebands in magic-angle spinning nuclear magnetic resonance: General principles and analytical solutions, *J. Chem. Phys.* **100,** 130–140 (1994).

36. A. Hagemeyer, D. van der Putten, and H. W. Spiess, The use of composite pulses in the TOSS experiment, *J. Magn. Reson.* **92,** 628–630 (1991).

37. B. Blümich, A. Hagemeyer, K. Schmidt-Rohr, and H. W. Spiess, Ultra-slow molecular motion in polymers: 1D and 2D NMR spectroscopy, *Ber. Bunsenges. Phys. Chem.* **93,** 1189–1193 (1989).